A summer heatwave reduced activity, heart rate and autumn body mass in a cold-adapted ungulate

L. Monica Trondrud[1*], Gabriel Pigeon[1,2], Elżbieta Król[3], Steve Albon[4], Erik Ropstad[5], Jouko Kumpula[6], Alina L. Evans[7], John R. Speakman[3,8,9.10] and Leif Egil Loe[1]

[1]Faculty of Environmental Sciences and Natural Resource Management, Norwegian University of Life Sciences, NO-1432 Ås, Norway

[2]Institut de recherche sur les forêts, Université du Québec en Abitibi-Témiscamingue, J9X 5E4, Rouyn-Noranda, Québec, Canada.

[3]School of Biological Sciences, Institute of Biological and Environmental Sciences, University of Aberdeen, Aberdeen, AB24 2TZ, UK

[4] The James Hutton Institute, Craigiebuckler, Aberdeen AB15 8QH, UK4

[5] Faculty of Veterinary Science, Norwegian University of Life Sciences, NO-1432 Ås, Norway.

[6]Wildlife ecology, Natural Resources Institute Finland, FIN-999870, Inari, Finland

[7]Department of Forestry and Wildlife Management, Inland Norway University of Applied Sciences, Campus Evenstad, Elverum, Norway

[8]Shenzhen Key Laboratory for Metabolic Health, Center for Energy Metabolism and Reproduction, Institute of Biology and Biotechnology, Shenzhen Institutes of Advanced Technology, CAS, Shenzhen, China

[9]CAS Center of Excellence in Animal Evolution and Genetics, Kunming, China

[10]State Key Laboratory of Molecular Developmental Biology, Institute of Genetics and Developmental Biology, CAS, Beijing, 100101, China

*Corresponding author: L. Monica Trondrud (monica.trondrud@nmbu.com; monica.trondrud@gmail.com)

Keywords: climate change, biologging, reproduction, thermoregulation, heat dissipation, ruminants, behavioural plasticity

What is already known

Endotherms buffer heat stress through physiological and behavioral adjustments. External or internal constraints in these responses can negatively impact fitness and adaptation to warmer conditions.

What this study adds

Integrated physiological and behavioral response to a severe, natural heatwave with subsequent, negative consequences for autumn body mass in a cold-adapted ungulate facing rapid climate change.

Abstract

Heatwaves are becoming more frequent across the globe and may impose severe thermoregulatory challenges for endotherms. Heat stress can induce both behavioral and physiological responses, which may result in energy deficits with potential fitness consequences. We studied the responses of reindeer (*Rangifer tarandus tarandus*), a cold-adapted ungulate, to a record-breaking heatwave in Northern Finland. Activity, heart rate, subcutaneous body temperature and body mass data were collected for 14 adult females. The post-heatwave autumn body masses were then analyzed against longitudinal body mass records for the herd from 1990 to 2021. With increasing air temperature during the day, reindeer became less active, had reduced heart rate and increased body temperature, reflecting both behavioral and physiological responses to heat stress. Although they increased activity in the late afternoon, on the hottest days (daily mean temperature ≥ 20°C), they failed to compensate for lost foraging time, and total time active was reduced by 9%. After the heatwave, the mean September body mass of herd females (69.7±6.6 kg, n = 52) was on average 16.4±4.8% lower than predicted (83.4±6.0 kg). Among focal females, individuals with the lowest levels of activity during the heatwave had the greatest mass loss over summer. We show how heatwaves impose a thermoregulatory challenge on endotherms, resulting in mass loss, potentially due to loss of foraging time. While it is well known that environmental conditions affect large herbivore fitness indirectly through decreased forage quality and limited water supply, direct effects of heat may be increasingly common in a warming climate.

Introduction

Climate change is happening at an unprecedent rate and is particularly pronounced in the polar regions (IPCC et al. 2019; Rantanen et al. 2022). There is also evidence of an increase in the occurrence of heatwaves in the terrestrial Arctic (Dobricic et al. 2020). Extreme high temperature events may pose a thermoregulatory challenge for endotherms since dissipation of body heat becomes more difficult (Schmidt-Nielsen 1997; Speakman and Król 2010), especially for cold-adapted species (Brivio et al. 2019) and lactating females (Zhao et al. 2020). To reduce the risk of hyperthermia under hot environmental conditions, endotherms employ thermoregulatory responses that can be energetically costly (McNab 2002), and/or they reduce activity, which impacts energy acquisition and allocation (Speakman and Król 2010; van Beest and Milner 2013). How cold-adapted animals cope under high environmental temperatures, and the consequences of their responses, may affect their growth, development and ultimately fitness in a rapidly warming climate (Stillman 2019).

Avoiding, or reducing, the risk of hyperthermia may involve several behavioral and physiological adjustments. For example, animals may seek cooler microclimates to reduce radiant heat loads and increase convective heat loss (Mitchell et al. 2018), modify peripheral blood flow to elevate skin/surface temperatures (Irving and Krog 1955) or employ evaporative cooling, via increased panting or sweating (Parker and Robbins 1984). Among ungulates, the use of thermal refugia such as forest canopies providing shade (van Beest et al. 2012), cool ground (Williamsen et al. 2019), or snow patches (Sarmento et al. 2019), can be an effective buffer against heat stress. Other responses include lowering food intake (Shively et al. 2019), and reductions in exercise intensity or movement rates (Brivio et al. 2019; Zhou et al. 2022). Also, spending less time foraging during the hottest part of the day and increasing foraging activity at dawn and/or dusk, as documented in temperate, alpine and desert ungulates (Aublet et al. 2009; Shrestha et al. 2014; Ditmer et al. 2018), can reduce heat

load without compromising overall foraging time (Semenzato et al. 2021). However, if temperatures remain high for long periods, or animals are unable to adopt alternative foraging patterns, behavioral buffering of heat stress may be insufficient and could potentially lead to lowered energetic investment in somatic growth (van Beest and Milner 2013) and depressed reproductive output (Igono et al. 1992; Dash et al. 2016). Indeed, it has been suggested that, in mammals, the ability to dissipate body heat is a key factor limiting energy expenditure (Speakman and Król 2010).

Reindeer (*Rangifer tarandus*) are large ungulates with a circumpolar distribution in the Northern Hemisphere. They are the only cervids with a long history of domestication and are an important livestock in local communities and indigenous traditions in Fennoscandia and Siberia (Røed et al. 2008). With their relatively large body size and highly insulating pelage, reindeer are well adapted to the cold, Arctic climate. Their thermoregulatory adaptations are efficient at saving water and retaining body heat in the cold while maximizing heat dissipation when hot (Folkow and Mercer 1986; Johnsen et al. 1990). In captivity, resting reindeer in their summer coats begin to show signs of heat stress (thermal tachypnea) at air temperatures exceeding 25°C (Blix and Johnsen 1983). Furthermore, reindeer fed *ad libitum* reduce their dry matter intake as air temperatures increase in summer (Thompson and Barboza 2014). Although this suggests that reindeer may be susceptible to heat stress during summer, little is known about the ability of reindeer to cope with sporadic extreme heat events under natural conditions.

In the summer of 2018, Northern Europe experienced a record-breaking heatwave causing droughts and wildfires (Peters et al. 2020). The heatwave in Scandinavia lasted 21 days (Kueh and Lin 2020), during which several areas above the Arctic circle (66°N) recorded the highest temperature anomalies since 1961. In Northern Finland (Inari region), the monthly mean temperature in July was 19.2°C, which was 5.1°C higher than the

climatological mean for this region, with anomalous high air pressure and little precipitation (Sinclair et al. 2019). Here, we investigate the behavioral and physiological responses of semi-domesticated reindeer (*R. t. tarandus*) during the 2018 heatwave. In response to higher air temperatures, we expected that adult female reindeer would reduce activity levels (Prediction 1), particularly in the hottest part of the day, and then compensate this reduction by increasing activity in the cooler parts of the day (Semenzato et al. 2021). In addition, we expected that females with calves would spend more time active (i.e. foraging) than females without a calf, due to the energetic demands of lactation (Denryter et al. 2020). We also anticipated that reindeer would exhibit increased resting heart rate and subcutaneous body temperature (Prediction 2), to facilitate heat dissipation via peripheral vasodilation and hence thermal conduction through the skin. Further, we expected that females with calves would display more pronounced thermoregulatory responses to alleviate heat stress, at lower air temperature thresholds, in accordance with the heat dissipation limitation theory (Speakman and Król 2010). Lastly, we predicted that females unable to compensate their energy needs due to reduced (or lost) foraging time in summer would have lower body mass in autumn (Prediction 3; van Beest and Milner 2013), and expected that variation in mean annual body mass over three decades would correlate with prevailing summer temperatures.

Methods

Animals and study area

Reindeer at the Kutuharju Reindeer Research Facility (Kaamanen, Northern Finland, 69° 8' N, 26° 59' E, Fig. A1-1, available online) consist of a herd of ~100 animals, belonging to the Reindeer Herders' Association. The herding management included keeping reindeer in two large enclosures (~13.8 and ~15 km^2) after calving until the rut, after which animals were moved to a winter enclosure (~15 km^2), and then in spring to a calving paddock (~0.3 km^2) to give birth (see Appendix 1, available online, for further details on the study area). The herd graze freely on natural pastures from May to November after which they are provided with silage and pellets as a supplementary feed in winter. During the period from September to April animals are weighed monthly by being gathered from the large enclosures and into the calving paddock. From here they are corralled and guided individually to an indoor handling facility containing a caged floor scale, which the reindeer walk onto to be weighed.

The study involved biologging 14 reindeer females from the Kutuharju herd (Focal animals: Table A1-1) in the summer of 2018. Ten of these individuals had been confined to the calving paddock and handled repeatedly in the period 31 May to 16 June, prior to the present study, as part of energetics study using the doubly labelled water technique (Trondrud 2021). During this period, they received supplemental feeding. They were let out on natural pasture with the rest of the herd on 17 June. For the analyses of activity, heart rate and body temperature, we used data collected in the period 20 June to 20 August to exclude the period when 10 of the 14 individuals were repeatedly handled, while still capturing the heat wave period (Fig. 1). There were negligible differences between the two groups in all aspects of the analyses described below (details in Appendix 2, available online).

Heart rate (HR) and subcutaneous body temperature (T_{sc}) data

In February 2018, the focal females were instrumented with a heart rate (HR) and temperature logger (DST centi-HRT, Star-Oddi, Gardabaer, Iceland). The surgical protocol is described in Appendix 1, available online. The DST centi-HRT sensors recorded HR and subcutaneous body temperature (T_{sc}) every 15 min. HR was automatically calculated from a 4-sec electrocardiogram (ECG) at 150 Hz measurement frequency, alongside an index for signal quality. Additional data processing is described in Appendix 1.

Activity data

The animals were fitted with collar-mounted tri-axial accelerometers (Vertex Plus Activity Sensor, Vectronic Aerospace GmbH, Berlin, Germany) to monitor their activity levels. These sensors recorded acceleration (*g*) in three directions representing back-forward, lateral, and dorsal-ventral movements at 8 Hz resolution. For each axis, partial dynamic body acceleration (PDBA) was calculated by subtracting the static acceleration using a 4 sec running average from the raw acceleration (Shepard et al. 2008). We estimated vectorial dynamic body acceleration (VeDBA) by calculating the square root of the sum of squared PDBAs (Wilson et al. 2020). We aggregated VeDBA data into 15-min sums (hereafter "sum VeDBA") to match with HR and T_{sc} records. Corrections for time offsets are described in Appendix 1.3. Due to battery failure in four of the DST centi-HRTs, only 10 of the 14 individuals had complete data from both loggers (activity and heart rate).

Weather and climate data

We set up a local HOBO weather station (Onset Computer Corporation, Bourne, MA, USA) mounted on a 2 m tall tripod in May 2018 that measured air temperature (T_a, °C) at 15-minute intervals. The placement of the station was between the two summer paddocks. These measurements were matched to the nearest timestamps for VeDBA, HR and T_{sc} recordings. Also, we obtained weather records from the nearest public weather stations for the years

1990–2021 (Table A1-2). Weather station IDs and locations relative to the study area are shown in Fig. A1-1.

Body mass of reindeer

We used April and September body masses of adult females (3–15 years) and their calves in the Kutuharju herd collected between 1990 and 2021 (Tables A1-3 and A1-4). Because this is a research herd, some individuals have been part of experimental feeding programs in the past, and therefore not included in body mass analyses. Since 1990, a total of 1519 September body masses were used, from 344 unique individuals. The median number of records (i.e., years weighed) per individual was 5 (range 1–13).

Statistical analyses

All statistical analyses were conducted in R version 4.1.1 (The R Core Team 2021). Mean values are presented with standard deviation (SD), and parameter estimates with standard error (SE).

We fitted hidden Markov models (HMM) to 15-min sum VeDBA using the package 'momentuHMM' (McClintock and Michelot 2018). HMMs assume that the observed pattern is driven by an underlying latent state sequence (a finite Markov chain). These states can then be used as proxies to interpret the animal's unobserved behavior (Langrock et al. 2012). We assumed only two underlying states, thought to represent 'inactive' (i.e., resting) and 'active' (Fig. A1-3). The 'active' state thus contains multiple forms of movement, e.g., foraging, walking, and running, but reindeer spend more than 50% of the time foraging in summer (Skogland 1980). We fitted several HMMs to evaluate both external (temperature and time of day) and individual-level (calf status) effects on the probability to occupy each state (stationary state probabilities). The combination of the explanatory variables in each HMM is listed in Appendix 1, Table A1-5. T_a was fitted as a continuous variable with piecewise

polynomial spline with 8 knots, asserted from visual inspection of the model outputs. We included sine and cosine terms for time of day to account for cyclicity. In addition, to assess the impact of T_a on activity patterns, we fitted five temperature-day categories, together with an interaction with time of day. These categories were based on quintiles (20% intervals) of the distribution of temperature data from our local weather station, in the period 20 June to 20 August 2018, with ranges of < 10°C (cold), 10−13°C (cool), 13−16°C (intermediate) 16−20°C (warm) and ≥ 20°C (hot). We evaluated the significance of each variable on the stationary state probabilities from the confidence intervals of each estimate, and the goodness-of-fit of each model using Akaike information criteria (AIC; Burnham and Anderson 2002), retaining models within $\Delta AIC < 5$. We extracted the most likely state occupied by an individual using the *Viterbi* function, returning the optimal state pathway, i.e., a two-level categorical variable indicating whether the individual was *most likely* resting or active. We used this output to calculate daily activity budgets (% time spent active).

We matched the activity states derived from the HMM to the HR and T_{sc} data. We opted to investigate the drivers of variation in HR and T_{sc} within the inactive state only, to simplify analyses. HR and T_{sc} were fitted as response variables in separate generalized additive mixed-effects models (GAMM), which included the following smooth terms: calendar day as a thin-plate regression spline, time of day (ToD, in hours, knots [*k*] = 10) as a cubic regression spline and individual as random intercept. All models were fitted using restricted maximum likelihood, a penalization value (λ) of 1.4 (Wood 2017), and an autoregressive structure (AR1) to account for temporal autocorrelation. We used the '*gam.check'* function from the 'mgcv' package to select *k*. The sum of VeDBA in the past 15 minutes was included as a predictor in all models. All models were fitted with the same set of explanatory variables: sum VeDBA, age, body mass (BM), calf status (Y/N), T_a, as well as interactions between calf status and T_a, and BM and T_a. The models were initially fitted with

the same explanatory variables using maximum likelihood, and simplified through a stepwise backward model selection approach, with a likelihood ratio test performed at each removal step. In both models, age was the only variable that fell out and was removed from the final models (Table A1-6).

To investigate if the heatwave in the summer of 2018 affected subsequent body mass change, we fitted a GAMM using September body mass as the response variable, with calf status (Y/N), April body mass, and age (range 3–15 years) as a thin-plate regression spline, as predictor variables. Individual ID and year were included as random intercepts. This model was fitted using data for all years (1990-2021). We included the following environmental variables in separate models: mean T_a in July, sum of days with daily mean $T_a \geq 20$ °C, cumulative degree days ≥ 20°C (i.e., sum of daily mean temperatures ≥ 20°C) from 1 June to 31 August, total precipitation (mm) from 1 June to 31 August, and interactions between precipitation and temperature variables. All models were run twice, excluding the body masses in 2018 in the second run. We compared models including environmental variables against the base model following the same approach as for adult body masses. We repeated the analysis for calf body masses in September, fitted with the following explanatory variables in the base: calf sex (F/M), calf birthweight, weight of mother in April, age of mother as a thin-plate regression spline, including ID of mother and year as random intercepts. Model selection was performed using AIC (Tables A1-11, A1-12 to A1-13).

Finally, we compared the change in body mass from April 2018 to September 2018 against the activity patterns recorded in summer 2018 for 13 individuals with available body mass data from both periods. We fitted linear regressions with average daily time spent in activity, the time spent active on the hottest days, and the difference in activity levels between the hottest days and intermediate days as the explanatory variable including an additive effect of having a calf. We evaluated the models using AIC (Table A1-14).

Results

Air temperature (T_a) characteristics of summer 2018 heatwave in Northern Finland

The summer of 2018 was exceptionally warm. Over the sampling period (20 June−20 August) observed T_a ranged from 4.4 to 30.5°C with highest daily mean T_a of 25.1°C, recorded on July 18 and 19. All but five days in July 2018 had daily mean T_a above the 30-year climate normal (1991−2020; 14.0°C; Fig. 1), and 15 of these days were at least 5°C higher than the 30-year average. In the summer of 2018, cumulative degree days above 20°C was 48.1°C in 2018 compared to a median of 2.7°C across all other years (range 0 – 23.7°C: Table A1-2), and a total of 16 days when the mean air temperature exceeded 20°C ('hot days') compared with a median of 2 days. From the local weather station, instantaneous (15-min) temperatures peaked between 11:00 and 16:00 for all daily temperature categories (Fig. 2a).

Prediction 1: changes in activity levels in response to rising air temperature (T_a)

Two of the HMMs explained similar amounts of the variation in state probabilities in reindeer (Table A1-5). The first HMM contained time of day, ID, and calf status interactions with T_a (AIC weights = 0.74). The probability of being active was stable between 5 and 20°C and decreased curvilinearly as T_a continued to increase beyond 20°C (Fig. 3a). Overall, females with calves had a higher probability of being active at temperatures between 5 and 20°C than females without calves, but this difference disappeared when T_a exceeded 20°C.

The second-best HMM contained a time-of-day interaction with T_a categories (AIC weights = 0.26 and ΔAIC = 2). This model showed that reindeer displayed a diel activity pattern that shifted with increasing temperatures, with no differences between females with and without calves. Overall, the probability of being active was highest during midday on the coldest days (mean T_a < 10°C, and 10−13°C), but with a relatively weak diel pattern (Fig.

2b). The diel pattern became more pronounced on days with higher mean daily T_a, with a reduced probability of being active during the hottest part of the day, followed by the increased probability of being active in the cooler parts of the evening (Fig. 2b). As predicted, this compensation resulted in similar daily activity budgets, with animals being on average active for 63.4% (< 10°C), 63.7% (10−13°C), 64.4% (13−16°C), and 63.9% (16−20°C) of the day (Fig. 2c). However, on the hottest days (mean Ta > 20°C) activity levels were strongly reduced in the morning and the evening activity peaks were attenuated (Fig. 2c), resulting in a reduction in daily activity budgets to 58.0% (9% change).

Prediction 2: changes in subcutaneous body temperature (T_{sc}) and heart rate (HR)

As expected, reindeer T_{sc} increased linearly as T_a rose (Fig. 3b). While the slopes were significantly different between females with and without calves, the difference was small (Table A1-7). Across the whole range of observed T_a (from 4.4 to 30.5°C), T_{sc} varied by 2.1°C and 1.6°C for females with and without calves, respectively. In contrast to our prediction, resting HR declined as air temperatures rose (Fig. 3c, Table A1-8), and this response was significantly steeper in females with calves: for every 1°C increase in T_a, HR declined by 0.5 beats per minute (bpm) for females with calves, and by 0.3 bpm for females without calves. Across the observed T_a range, predicted resting HR declined from 77 to 63 bpm in females with calves and from 66 to 59 bpm in females without calves. The difference between the females with and without calves was therefore greatest at low T_a (mean difference of 11 bpm at T_a = 4°C) but differed by only 4 bpm at the highest T_a. For both T_{sc} and HR, we found significant interactions between T_a and body mass (Tables A1-7 and A1-8), where heavier females tended to have higher T_{sc} at low T_a but lower T_{sc} at high T_a, compared to lighter females. However, the effect size of the interaction was small with large overlapping confidence intervals for the predictions (Fig. A1-9a). For heart rate, heavier

females tended to have slightly lower heart rates at low T_a, but this difference disappeared as T_a increased (Fig. A1-9b).

Prediction 3: effects of summer 2018 heatwave on autumn body mass

The mean adult female body mass of the herd in September 2018 (69.7 ± 6.6 kg, n = 52), was the lowest recorded over the years 1990–2021 (Fig. 4a, Table A1-3). Calf status, age, and April body mass together with random effects for ID and year, explained 87.5% of the variation in September body mass over the 32 years (Table A1-9). On average, having a calf reduced September body mass by ~3.9 kg. Using this model to calculate the expected body mass for individuals in September 2018, we found that these were on average 16.4 ± 4.8% lower than expected (expected mean of 83.4 ± 6.0 kg). Further, we found a significant negative association between cumulative degree days and September body mass of herd females across the years 1990-2021 (Tables A1-10 and A1-11). However, when excluding data from 2018, the models containing any summer weather variable were indistinguishable from the null model, emphasizing that 2018 was an exceptional year in terms of both body mass patterns and weather extremes (Fig. 4b). Also in 2018, calves were on average 6.5 ± 3.0 kg (15 ± 6.6%) lighter than expected (43.7 ± 2.9 kg, Table A1-12), while none of the models containing environmental variables outperformed the null model (Table A1-13).

Among the 14 focal animals for which we had activity data, we had body masses from both April and September for 13 individuals. Here, we found a positive association between absolute mass change (difference between April and September body mass) in 2018 and average activity levels over summer (slope = 1.0, SE = 0.4, p = 0.02), when including calf as an additive effect (slope= −6.3, SE = 2.6, p = 0.04; Fig. 4c). Although the effect was statistically significant, the model could not be distinguished from the null model (Table A1-14). In partial support of prediction 3, individuals who were less active in summer tended to

the greatest negative mass change from April to September in 2018 (Fig. 4c) when accounting for the effect of having a calf.

Discussion

Our data provide evidence of heat stress in semi-domesticated reindeer in Northern Finland during the unprecedented summer heatwave of 2018. At higher air temperatures, when reindeer were inactive their subcutaneous body temperature increased, while heart rates declined, a combination that may indicate a heat-related decline in food intake (Shively et al. 2019). Reindeer adjusted behaviorally to warm daytime temperatures by reducing their midday activity levels. They compensated for this reduction by being more active later in the day when it was cooler. However, above 20°C this compensation was incomplete, resulting in a potential loss of daily feeding time. Consequently, individuals that were less active during summer, had depressed weight gain in September. While some of this depressed body mass could be due to lower food quality in a warm and dry summer, we suggest that high heat loads may have contributed to this mass loss, operating through depressed activity level, reduced heart rate and increased body temperature. Since body mass influences reproduction and survival, we anticipate that more intense heatwaves may increasingly impact fitness in mammals.

Because behavioral responses to environmental change are considered less costly than physiological responses (Hetem et al. 2014), animals are expected to first display thermoregulatory behavior when faced with conditions outside their thermoneutral zone (Mitchell et al. 2018). Here, we demonstrate that reindeer reduced their activity levels when air temperatures exceeded 20°C, likely to, a) minimize heat production from being active and seek thermal refugia, such as shade and cool ground (Mitchell et al. 2018) and/or b) reduce food intake to reduce heat load from rumination (Thompson and Barboza 2014; Shively et al. 2019), although this may be confounded by decreased food quality coinciding with heat

(Turbill et al. 2011). On days when air temperatures exceeded 20°C only briefly around midday, reindeer compensated for lost foraging time by increasing activity in the cooler parts of the day, a response also seen in other temperate (van Beest and Milner 2013), alpine (Semenzato et al. 2021; Zhou et al. 2022), and desert (Hetem et al. 2012) ungulates. However, reindeer failed to compensate for the reduced midday activity on the very hottest days during the heatwave, resulting in an overall reduction of daily activity. Similar results have been found in male alpine Ibex (*Capra ibex*), where the need to thermoregulate on warm days resulted in individuals foraging in areas with poorer vegetation without subsequent behavioral compensation to make up for low quality forage (Mason et al. 2017). When animals are not able to compensate for lost feeding time, reduced daily activity and subsequently lower daily food intake may have detrimental consequences for fitness when facing long-lasting and chronically high heat loads (van Beest and Milner 2013; Fuller et al. 2021).

In addition, we found a negative association between heart rate and increasing air temperatures in summer, but we did not observe a breakpoint similar to that in activity patterns, nor that shown for reindeer in captivity at around 25°C (Blix and Johnsen 1983). A decline in heart rate with increasing ambient temperature has also been documented in free-ranging moose (*Alces alces*; Thompson et al., 2020) and Svalbard reindeer (*R. t. platyrhynchus;* Trondrud et al. 2021), as well as in cattle (*Bos* spp.) in metabolic chambers (Beatty et al. 2006; de Andrade Ferrazza et al. 2017). Reductions in heart rate could be explained by an increased water intake which would subsequently increase blood volume and result in a higher stroke volume (Beatty et al. 2006; Thompson et al. 2020). Although the reindeer in our study had free access to drinking water via streams and small lakes, we did not have the means to quantify water consumption. However, in captive reindeer, dry matter intake has been found to decline linearly with increasing T_a (Thompson and Barboza 2014),

and both heart rate and activity patterns are associated with dry matter intake in reindeer (Mesteig et al. 2000; Nilsson et al. 2006). The reduction in activity levels, coupled with lower resting heart rate at higher air temperature, may suggest that reindeer obtained less food, or food of poorer quality, on the hottest days during the summer.

In contrast to the response of heart rate, we found a positive relationship between subcutaneous body temperature and air temperatures. This is unsurprising as peripherally measured body temperatures, such as of skin, typically display more variation than core body temperature (Schmidt-Nielsen 1997; Lust et al. 2007), and also fluctuate more with variation in T_a (Arnold et al. 2004; Brinkmann et al. 2012). At the highest recorded air temperatures, however, subcutaneous temperature approached values close to core body temperatures in reindeer (~38°C; Blix and Johnsen 1983), which may indicate that animals were at risk of developing hyperthermia. On the other hand, the main avenues of heat loss in resting reindeer during summer are through convection and radiation, and about 50% of radiant heat loss occurs via the trunk (Folkow and Mercer 1986). Increases in subcutaneous temperatures may therefore have facilitated heat loss to the environment via vasodilation, to defend against increases in core body temperature, a mechanism often employed by desert ungulates (Fuller et al. 2010).

The higher activity levels and resting heart rates in females with calves at low and intermediate air temperatures, compared to those without calves, suggests that females with calves had higher energy demands, likely due to the high energetic costs of lactation (Bårdsen et al. 2009). Our results are similar to those found in Svalbard reindeer (Trondrud et al. 2021). Although the apparent threshold of air temperature at which activity levels began to decline was similar for both groups (~20°C), females with calves reduced heart rate to a greater extent than females without calves (Fig. 3c). Despite similar responses in activity levels and subcutaneous body temperature, the steeper response in heart rate could indicate

that females with calves were more susceptible to heat stress (Speakman and Król 2010). Indeed, lactating females can be particularly sensitive to heat stress during the late lactational period (Zhao et al. 2020). The energetic demand of lactation can lead to reduced somatic growth in female ungulates compared to females who do not reproduce that year (Pigeon et al. 2022). In our herd, having a calf reduced September body mass by almost 4 kg. Additional constraints on food intake, via environmental heat load, may therefore be of greater consequence for females who reproduce, by further constraining the trade-off between investment into reproduction and maintenance.

In 2018 the September body masses were the lowest recorded in the past 32 years. Environmental conditions in both spring and summer impact autumn body mass in several ungulate species, presumably via changes in forage availability and insect harassment (Aanes et al. 2002; Hurley et al. 2014; Desforges et al. 2021; Johnson et al. 2022). In particular, poor spring conditions and large-scale climatic oscillations may result in lower autumn body masses (Holmes et al. 2021) and reduced population growth (Aanes et al. 2002). On the other hand, warmer temperatures in summer can also be associated with increased autumn body mass as shown in Svalbard reindeer (Albon et al. 2017). Insect harassment may also negatively impact body condition, often in interactions with temperature (Mörschel and Klein 2011) and nutritional quality (Johnson et al. 2022). Although the relationship between body mass and the prevailing weather during summer was weak when excluding the year 2018, the extreme contrast between this and other years is remarkable. Indeed, both recruitment and mass of Swedish moose calves was also reported to be considerably lower in 2018 (Holmes et al. 2021), which was attributed to low forage quality and availability. The exceptionally low body masses in 2018 of the reindeer in our study were likely caused by a combination of multiple environmental factors, including low forage quality due to low precipitation and poor spring conditions, insect harassment and air temperatures (see e.g. Mörschel and Klein

1997). Based on our findings, we suggest that high environmental heat loads during the summer of 2018 also contributed to the low body masses via changes in activity patterns and foraging effort to avoid heat stress. This suggestion is corroborated by our subset of females with activity data, for which we found a positive association between body mass change over summer and activity levels, providing a potential explanation for the lower body masses observed in September 2018. Although there is evidence that reindeer females in captivity can re-gain fat reserves after weaning their calves (Chan-McLeod et al. 1999), such compensations demand that sufficient food is available. In our study, supplementary feeding in the winter likely alleviated the consequence of reduced mass in 2018, as they had relatively high body masses the subsequent year (Fig. A1-8). The effects of restricted foraging in summer are therefore more likely to have a greater impact for wild ungulates (with natural sources of food) than in managed herds or domestic livestock that rely on food supplementation.

In recent decades there have been more frequent and intense heatwaves across the globe (IPCC, 2019). Acute heat stress can have detrimental effects on wildlife through mass mortalities, which in large mammals is typically due to dehydration or lack of food (Cheng, 2022; Young, 1994). However sub-lethal, chronic heat stress could lead to alterations in individual behavior, physiology and hence fitness, and consequently impact population dynamics (Conradie et al. 2019). We show that reindeer displayed behavioral and physiological signs of heat stress avoidance, under environmental temperatures that are predicted to become more common in the Arctic (IPCC et al. 2019). While behavioral responses have been documented in a wide array of mammalian species, few have investigated the simultaneous response in physiological parameters, and subsequent consequences for body mass. Our study emphasizes the importance of a better integration of behavior, physiology, and ecology when investigating animal responses to extreme

environmental conditions (Buckley and Huey 2016; Stillman 2019), all of which potentially influence the capacity of individuals to cope with a warming climate (Hetem et al. 2014; Fuller et al. 2021).

Author contributions. LEL, ALE, ER, JRS, EK and LMT planned the study. JK facilitated the field work, and ER, ALE, LMT, JK and LEL conducted the fieldwork including device deployment, retrieval, and animal handling. LMT curated and analysed the data together with GP. LMT drafted the manuscript, with input from SA. All authors contributed to editing and approved the final version of the manuscript.

Acknowledgements. We are grateful for the feedback from Robyn Hetem and two anonymous reviewers for their constructive inputs. We thank Clare Stawski and Murray M. Humphries for commenting on an earlier version of this work. Field work would not be possible without the collaboration with the Reindeer Herders' Association and local support from Mika Tervonen, Unto Paadar and Jukka Siitari, and field assistants Elise Tjørnsletten, Kine Øren and Erlend Søby. Veterinarians Marja Nourgam and Amanda Høyer Boesen contributed to the anaesthesia and surgery of the reindeer. We thank Asgeir Bjarnason at Star-Oddi LTD for help and guidance with biologger programming and data processing, and Larissa Beumer for advice on the HMM approach. Cassandra Ugland validated the HR measurements. The work was supported by the Norwegian Research Council grant number 267613 and 315454.

Ethics. The prior authorisation for all procedures carried out on the reindeer in this study was granted by the Animal Experiment Board at the Regional State Administrative Agency in Finland (license: ESAVI/3857/04.10.07/2017).

Data availability. Long-term climatic data is publicly available from the Finnish Meteorological Institute (https://en.ilmatieteenlaitos.fi/download-observations/). Curated biologger data and locally recorded weather data are available here: https://figshare.com/s/c1044ce71c363ccc20b8. The historical body mass data of females have been collected from the experimental reindeer herd at the Kutuharju Research Station by Finnish Reindeer Herders' Association, who also own the reindeer herd and the station (https://www.luke.fi/en/research/research-infrastructures/kutuharju-research-infrastructure). Natural Resources Institute Finland (Luke) updates, saves and administrates this long-term reindeer herd data.

Literature cited

Aanes R., B.E. Sæther, F.M. Smith, E.J. Cooper, P.A. Wookey, and N. Areøritsland. 2002. The Arctic Oscillation predicts effects of climate change in two trophic levels in a high-arctic ecosystem. Ecol Lett 5:445–453.

Albon S.D., R.J. Irvine, O. Halvorsen, R. Langvatn, L.E. Loe, E. Ropstad, V. Veiberg, et al. 2017. Contrasting effects of summer and winter warming on body mass explain population dynamics in a food-limited Arctic herbivore. Glob Change Biol 23:1374–1389.

Arnold W., T. Ruf, S. Reimoser, F. Tataruch, K. Onderscheka, and F. Schober. 2004. Nocturnal hypometabolism as an overwintering strategy of red deer (Cervus elaphus). Am J Physiol - Regul Integr Comp Physiol 286:R174–R1811.

Aublet J.-F., M. Festa-Bianchet, D. Bergero, and B. Bassano. 2009. Temperature constraints on foraging behaviour of male Alpine ibex (Capra ibex) in summer. Oecologia 159:237–247.

Bårdsen B.J., P. Fauchald, T. Tveraa, K. Langeland, and M. Nieminen. 2009. Experimental evidence of cost of lactation in a low risk environment for a long-lived mammal. Oikos 118:837–852.

Beatty D.T., A. Barnes, E. Taylor, D. Pethick, M. McCarthy, and S.K. Maloney. 2006. Physiological responses of Bos taurus and Bos indicus cattle to prolonged, continuous heat and humidity. J Anim Sci 84:972–985.

Blix A.S. and H.K. Johnsen. 1983. Aspects of nasal heat exchange in resting reindeer. J Physiol 340:445–454.

Brinkmann L., M. Gerken, and A. Riek. 2012. Adaptation strategies to seasonal changes in environmental conditions of a domesticated horse breed, the Shetland pony (Equus ferus caballus). J Exp Biol 215:1061–1068.

Brivio F., M. Zurmühl, S. Grignolio, J. von Hardenberg, M. Apollonio, and S. Ciuti. 2019. Forecasting the response to global warming in a heat-sensitive species. Sci Rep 9:1–16.

Buckley L.B. and R.B. Huey. 2016. Temperature extremes: geographic patterns, recent changes, and implications for organismal vulnerabilities. Glob Change Biol 22:3829–3842.

Burnham K.P. and D.R. Anderson. 2002. Model Selection and Multimodel Inference: A Practical Information-Theoretic Approach (Vol. 172). Springer, New York.

Chan-McLeod A.C.A., R.G. White, and D.E. Russell. 1999. Comparative body composition strategies of breeding and nonbreeding female caribou. Can J Zool 77:1901–1907.

Cheng, Amy. 2022. Extreme heat and humidity kill thousands of cattle in Kansas. Wash Post.

Conradie S.R., S.M. Woodborne, S.J. Cunningham, and A.E. McKechnie. 2019. Chronic, sublethal effects of high temperatures will cause severe declines in southern African arid-zone birds during the 21st century. Proc Natl Acad Sci U S A 116:14065–14070.

Dash S., A.K. Chakravarty, A. Singh, A. Upadhyay, M. Singh, and S. Yousuf. 2016. Effect of heat stress on reproductive performances of dairy cattle and buffaloes: A review. Vet World 9:235–244.

de Andrade Ferrazza R., H.D. Mogollón Garcia, V.H. Vallejo Aristizábal, C. de Souza Nogueira, C.J. Veríssimo, J.R. Sartori, R. Sartori, et al. 2017. Thermoregulatory responses of Holstein cows exposed to experimentally induced heat stress. J Therm Biol 66:68–80.

Denryter K., R.C. Cook, J.G. Cook, K.L. Parker, and M.P. Gillingham. 2020. State-dependent foraging by caribou with different nutritional requirements. J Mammal 101:544–557.

Desforges J.-P., G.M. Marques, L.T. Beumer, M. Chimienti, L.H. Hansen, S.H. Pedersen, N.M. Schmidt, et al. 2021. Environment and physiology shape Arctic ungulate population dynamics. Glob Change Biol 27:1755–1771.

Ditmer M.A., R.A. Moen, S.K. Windels, J.D. Forester, T.E. Ness, and T.R. Harris. 2018. Moose at their bioclimatic edge alter their behavior based on weather, landscape, and predators. Curr Zool 64:419–432.

Dobricic S., S. Russo, L. Pozzoli, J. Wilson, and E. Vignati. 2020. Increasing occurrence of heat waves in the terrestrial Arctic. Environ Res Lett 15:024022.

Folkow L.P. and J.B. Mercer. 1986. Partition of heat loss in resting and exercising winter- and summer-insulated reindeer. Am J Physiol 251:R32–R40.

Fuller A., T. Dawson, B. Helmuth, R.S. Hetem, D. Mitchell, and S.K. Maloney. 2010. Physiological mechanisms in coping with climate change. Physiol Biochem Zool 83:713–720.

Fuller A., D. Mitchell, S.K. Maloney, R.S. Hetem, V.F.C. Fonsêca, L.C.R. Meyer, T.M.F.N. van de Ven, et al. 2021. How dryland mammals will respond to climate change: the effects of body size, heat load and a lack of food and water. J Exp Biol 224:jeb238113.

Hetem R.S., A. Fuller, S.K. Maloney, and D. Mitchell. 2014. Responses of large mammals to climate change. Temperature 1:115–127.

Hetem R.S., W.M. Strauss, L.G. Fick, S.K. Maloney, L.C.R. Meyer, M. Shobrak, A. Fuller, et al. 2012. Activity re-assignment and microclimate selection of free-living Arabian oryx: Responses that could minimise the effects of climate change on homeostasis? Zoology 115:411–416.

Holmes S.M., J.P.G.M. Cromsigt, K. Danell, G. Ericsson, N.J. Singh, and F. Widemo. 2021. Declining recruitment and mass of Swedish moose calves linked to hot, dry springs and snowy winters. Glob Ecol Conserv 27:e01594.

Hurley M.A., M. Hebblewhite, J.-M. Gaillard, S. Dray, K.A. Taylor, W.K. Smith, P. Zager, et al. 2014. Functional analysis of Normalized Difference Vegetation Index curves reveals overwinter mule deer survival is driven by both spring and autumn phenology. Philos Trans R Soc B Biol Sci 369:20130196.

Igono M.O., G. Bjotvedt, and H.T. Sanford-Crane. 1992. Environmental profile and critical temperature effects on milk production of Holstein cows in desert climate. Int J Biometeorol 36:77–87.

IPCC, H.-O. Pörtner, D.C. Roberts, V. Masson-Delmotte, P. Zhai, M. Tignor, E. Poloczanska, et al. 2019. *IPCC Special Report on the Ocean and Cryosphere in a Changing Climate*.

Irving L. and J. Krog. 1955. Temperature of Skin in the Arctic as a Regulator of Heat. J Appl Physiol 7:355–364.

Johnsen H.K., K.J. Nilssen, A. Rognmo, and A.S. Blix. 1990. Reindeer breathe less and save water in the cold. Rangifer 10:243–247.

Johnson H.E., E.A. Lenart, D.D. Gustine, L.G. Adams, and P.S. Barboza. 2022. Survival and reproduction in Arctic caribou are associated with summer forage and insect harassment. Front Ecol Evol 10.

Kueh M.T. and C.Y. Lin. 2020. The 2018 summer heatwaves over northwestern Europe and its extended-range prediction. Sci Rep 2020 101 10:1–18.

Langrock R., R. King, J. Matthiopoulos, L. Thomas, D. Fortin, and J.M. Morales. 2012. Flexible and practical modeling of animal telemetry data: hidden Markov models and extensions. Ecology 93:2336–2342.

Lust A., A. Fuller, S.K. Maloney, D. Mitchell, and G. Mitchell. 2007. Thermoregulation in pronghorn antelope (Antilocapra americana Ord) in the summer. J Exp Biol 210:2444–2452.

Mason T.H.E., F. Brivio, P.A. Stephens, M. Apollonio, and S. Grignolio. 2017. The behavioral trade-off between thermoregulation and foraging in a heat-sensitive species. Behav Ecol 28:908–918.

McClintock B.T. and T. Michelot. 2018. momentuHMM: R package for generalized hidden Markov models of animal movement. Methods Ecol Evol 9:1518–1530.

McNab B.K. 2002. The Physiological Ecology of Vertebrates: A View from Energetics. Cornell University Press, New York.

Mesteig K., N.J.C. Tyler, and A.S. Blix. 2000. Seasonal changes in heart rate and food intake in reindeer (Rangifer tarandus tarandus). Acta Physiol Scand 170:145–151.

Mitchell D., E.P. Snelling, R.S. Hetem, S.K. Maloney, W.M. Strauss, and A. Fuller. 2018. Revisiting concepts of thermal physiology: Predicting responses of mammals to climate change. J Anim Ecol 87:956–973.

Mörschel F.M. and D.R. Klein. 1997. Effects of weather and parasitic insects on behavior and group dynamics of caribou of the Delta Herd, Alaska. Httpsdoiorg101139z97-793 75:1659–1670.

Nilsson A., B. Åhman, H. Norberg, I. Redbo, E. Eloranta, and K. Olsson. 2006. Activity and heart rate in semi-domesticated reindeer during adaptation to emergency feeding. Physiol Behav 88:116–123.

Parker K.L. and C.T. Robbins. 1984. Thermoregulation in mule deer and elk. Can J Zool 62:1409–1422.

Peters W., A. Bastos, P. Ciais, and A. Vermeulen. 2020. A historical, geographical and ecological perspective on the 2018 European summer drought. Philos Trans R Soc B 375.

Pigeon G., S. Albon, L.E. Loe, R. Bischof, C. Bonenfant, M. Forchhammer, R.J. Irvine, et al. 2022. Context-dependent fitness costs of reproduction despite stable body mass costs in an Arctic herbivore. J Anim Ecol 91:61–73.

Rantanen M., A.Y. Karpechko, A. Lipponen, K. Nordling, O. Hyvärinen, K. Ruosteenoja, T. Vihma, et al. 2022. The Arctic has warmed nearly four times faster than the globe since 1979. Commun Earth Environ 3:1–10.

Røed K.H., Ø. Flagstad, M. Nieminen, Ø. Holand, M.J. Dwyer, N. Røv, and C. Vilà. 2008. Genetic analyses reveal independent domestication origins of Eurasian reindeer. Proc R Soc B Biol Sci 275:1849–1855.

Sarmento W., M. Biel, and J. Berger. 2019. Seeking snow and breathing hard – Behavioral tactics in high elevation mammals to combat warming temperatures. PLoS ONE 14:e0225456.

Schmidt-Nielsen K. 1997. Animal Physiology: Adaptation and Environment. Cambridge University Press.

Semenzato P., F. Cagnacci, F. Ossi, E. Eccel, N. Morellet, A.J.M. Hewison, E. Sturaro, et al. 2021. Behavioural heat-stress compensation in a cold-adapted ungulate: Forage-mediated responses to warming Alpine summers. Ecol Lett ele.13750.

Shepard E., R. Wilson, L. Halsey, F. Quintana, A. Gómez Laich, A. Gleiss, N. Liebsch, et al. 2008. Derivation of body motion via appropriate smoothing of acceleration data. Aquat Biol 4:235–241.

Shively R.D., J.A. Crouse, D.P. Thompson, and P.S. Barboza. 2019. Is summer food intake a limiting factor for boreal browsers? Diet, temperature, and reproduction as drivers of consumption in female moose. (N. Righini, ed.)PLOS ONE 14:e0223617.

Shrestha A.K., S.E. van Wieren, F. van Langevelde, A. Fuller, R.S. Hetem, L. Meyer, S. de Bie, et al. 2014. Larger antelopes are sensitive to heat stress throughout all seasons but smaller antelopes only during summer in an African semi-arid environment. Int J Biometeorol 58:41–49.

Sinclair V.A., J. Mikkola, M. Rantanen, and J. Räisänen. 2019. The summer 2018 heatwave in Finland. Weather 74:403–409.

Skogland T. 1980. Comparative summer feeding strategies of arctic and alpine rangifer. J Anim Ecol 49:81–98.

Speakman J.R. and E. Król. 2010. Maximal heat dissipation capacity and hyperthermia risk: Neglected key factors in the ecology of endotherms. J Anim Ecol 79:726–746.

Stillman J.H. 2019. Heat Waves, the New Normal: Summertime Temperature Extremes Will Impact Animals, Ecosystems, and Human Communities. Physiology 34:86–100.

The R Core Team. 2021. R: A language and environment for statistical computing. R Foundation for Statistical Computing, Vienna, Austria.

Thompson D.P. and P.S. Barboza. 2014. Nutritional implications of increased shrub cover for caribou (Rangifer tarandus) in the Arctic. Can J Zool 92:339–351.

Thompson D.P., J.A. Crouse, S. Jaques, and P.S. Barboza. 2020. Redefining physiological responses of moose (Alces alces) to warm environmental conditions. J Therm Biol 90:102581.

Trondrud L.M. 2021. *Energetics in seasonal environments: reindeer as a case study.* (PhD Dissertation). Norwegian University of Life Sciences, Ås.

Trondrud L.M., G. Pigeon, S. Albon, W. Arnold, A.L. Evans, R.J. Irvine, E. Król, et al. 2021. Determinants of heart rate in Svalbard reindeer reveal mechanisms of seasonal energy management. Philos Trans R Soc B Biol Sci 376:20200215.

Turbill C., T. Ruf, T. Mang, and W. Arnold. 2011. Regulation of heart rate and rumen temperature in red deer: Effects of season and food intake. J Exp Biol 214:963–970.

van Beest F.M. and J.M. Milner. 2013. Behavioural Responses to Thermal Conditions Affect Seasonal Mass Change in a Heat-Sensitive Northern Ungulate. PLoS ONE 8:e65972.

van Beest F.M., B. Van Moorter, and J.M. Milner. 2012. Temperature-mediated habitat use and selection by a heat-sensitive northern ungulate. Anim Behav 84:723–735.

Williamsen L., G. Pigeon, A. Mysterud, A. Stien, M. Forchhammer, and L.E. Loe. 2019. Keeping cool in the warming Arctic: thermoregulatory behaviour by Svalbard reindeer (Rangifer tarandus platyrhynchus). Can J Zool 97:1177–1185.

Wilson R.P., L. Börger, M.D. Holton, D.M. Scantlebury, A. Gómez-Laich, F. Quintana, F. Rosell, et al. 2020. Estimates for energy expenditure in free-living animals using acceleration proxies: A reappraisal. J Anim Ecol 89:161–172.

Wood S.N. 2017. Generalized Additive Models: An Introduction with R. Chapman and Hall/CRC.

Young T.P. 1994. Natural Die-Offs of Large Mammals: Implications for Conservation. Conserv Biol 8:410–418.

Zhao Z.-J., C. Hambly, L.-L. Shi, Z.-Q. Bi, J. Cao, and J.R. Speakman. 2020. Late lactation in small mammals is a critically sensitive window of vulnerability to elevated ambient temperature. Proc Natl Acad Sci 117:24352–24358.

Zhou W., M. Wang, K. Gao, H. Gao, F. Wei, and Y. Nie. 2022. Behavioural thermoregulation by montane ungulates under climate warming. Divers Distrib 00:1–10.

Figure Legends

Figure 1. Daily mean air temperatures (black line) recorded from a local weather station in summer of 2018 in Kaamanen, Northern Finland. The dark grey shading indicates the temperature amplitude for each day (daily maxima and minima). The light grey shading denotes the period during which activity, HR and T_{sc} were used in analysis of reindeer responses to environmental conditions (20 June – 20 August). The blue line indicates the daily mean air temperatures recorded between 1990 and 2021 by a weather station ~60 km from the study site (station ID 102033).

Figure 2. Air temperatures and mean activity levels of 14 adult female reindeer from 20 June to 20 August 2018 in Kaamanen, Northern Finland. a) Smoothed average air temperatures over 24 h for different daily mean T_a categories. b) Probability of being active over 24 h for different daily mean T_a categories estimated from a hidden Markov model. The lines show the predicted mean probability, and the shaded region represents the 95% credible interval for each prediction. c) Estimated daily activity budgets (% of time active) plotted over 24 h derived from the probability estimates of a hidden Markov model, grouped by different daily mean T_a categories and shown as smoothed averages across all individuals.

Figure 3. Responses of 10 adult female reindeer with calves (dark grey, triangles) and without calves (light grey, squares) to instantaneous air temperatures from 20 June to 20 August 2018 in Kaamanen, Northern Finland. a) Probability of being active predicted from HMM. b) Subcutaneous body temperatures (T_{sc}) predicted from GAMM. Points show adjusted means ± SEM. c) Predicted resting heart rates predicted from GAMM. Points show adjusted means ± SEM. In all panels, the shaded areas show the 95% confidence interval for each prediction, and fainted points outside the prediction represent the lower 1% and upper 99% of the data. All predictions and adjusted points are corrected for other explanatory variables in each model.

Figure 4. a) Median September body mass in adult reindeer females each year 1990-2021 (n = 1519, 344 individuals). 2007 was excluded due to insufficient data in unmanipulated individuals. Horizontal lines show the median and the lower and upper ends of the box correspond to the first and third quartiles, and whiskers extend to up to 1.5 times the inter-quartile range. b) September body mass across all years of available data (1990-2021, except 2007), as a function of cumulative degree days (sum of daily mean temperatures above 20°C). The points are adjusted for each female's age, April body mass and calf status. The line represents the predicted relationship between body mass and the cumulative degree days in summer when excluding the year 2018 (red point). c) Summer mass change (difference between April and September body mass) in 2018, against the mean activity level (%) over summer in 13 adult reindeer females with a calf (triangles) and without a calf (squares). The two lines represent the predicted response for females with a calf (solid line) and without (dashed line), derived from a linear regression with activity level and calf status as the predictors and summer mass change as the response (Adj. $R^2 = 0.41$, $p = 0.03$).

Figure 1

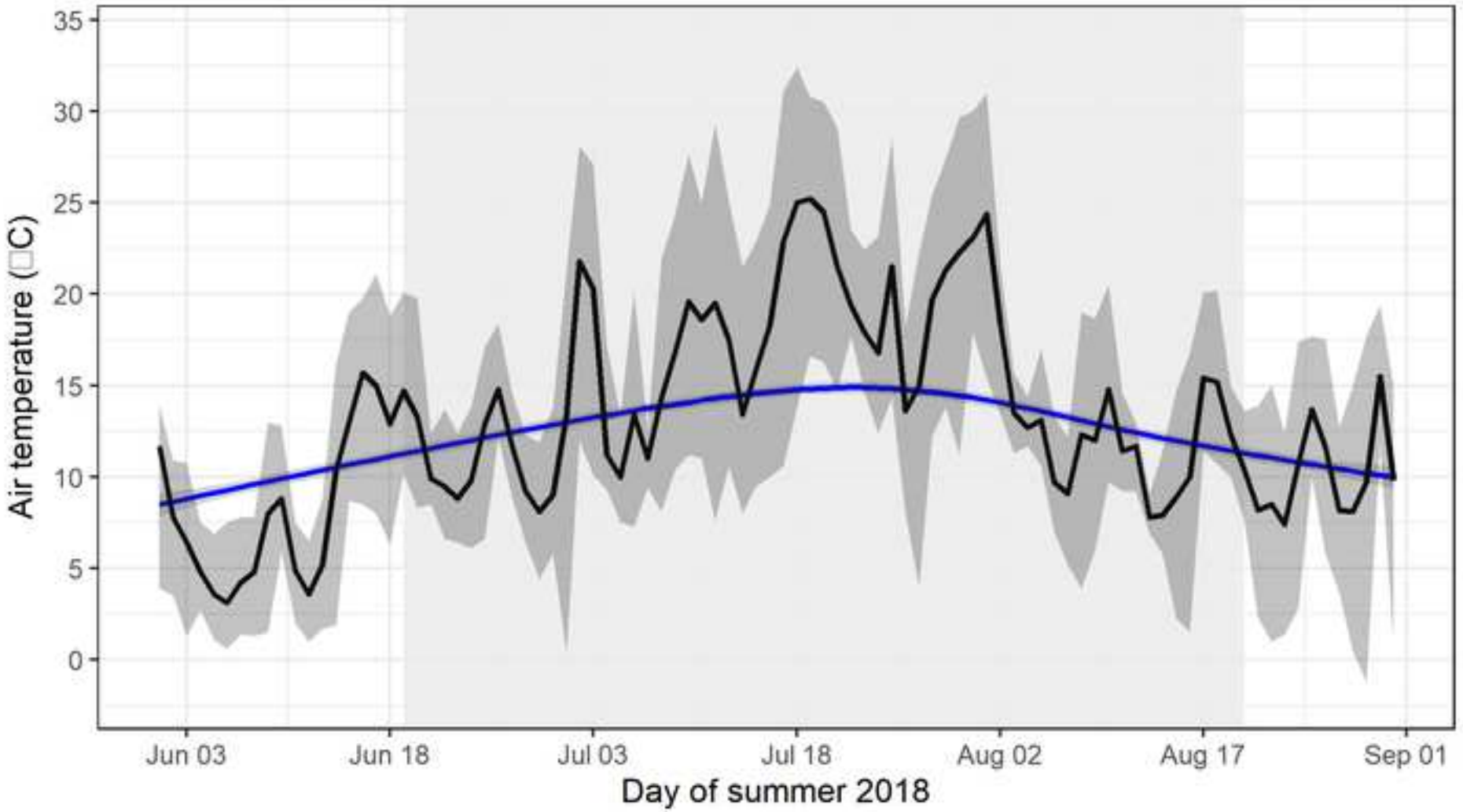

Figure 2

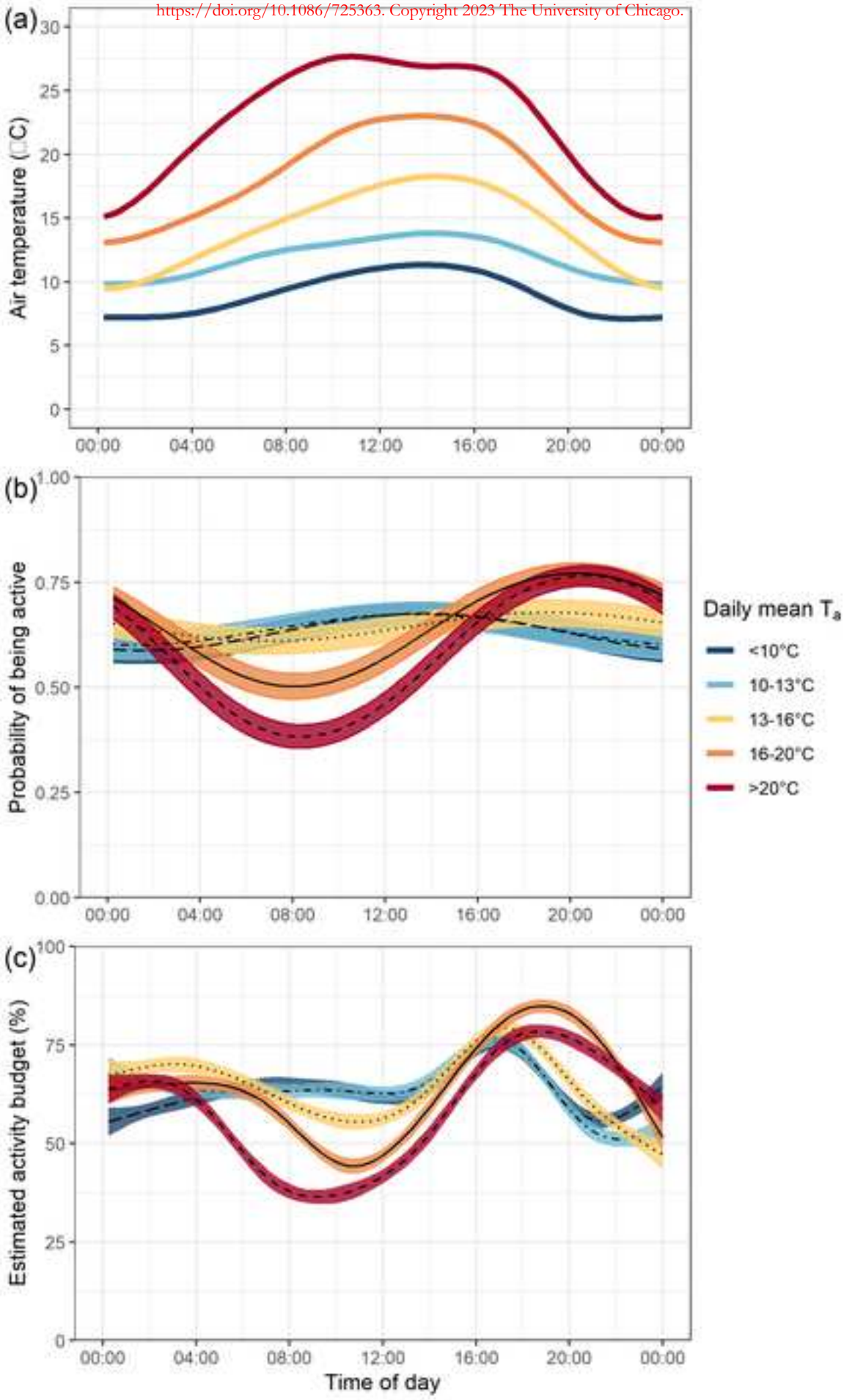

Figure 3

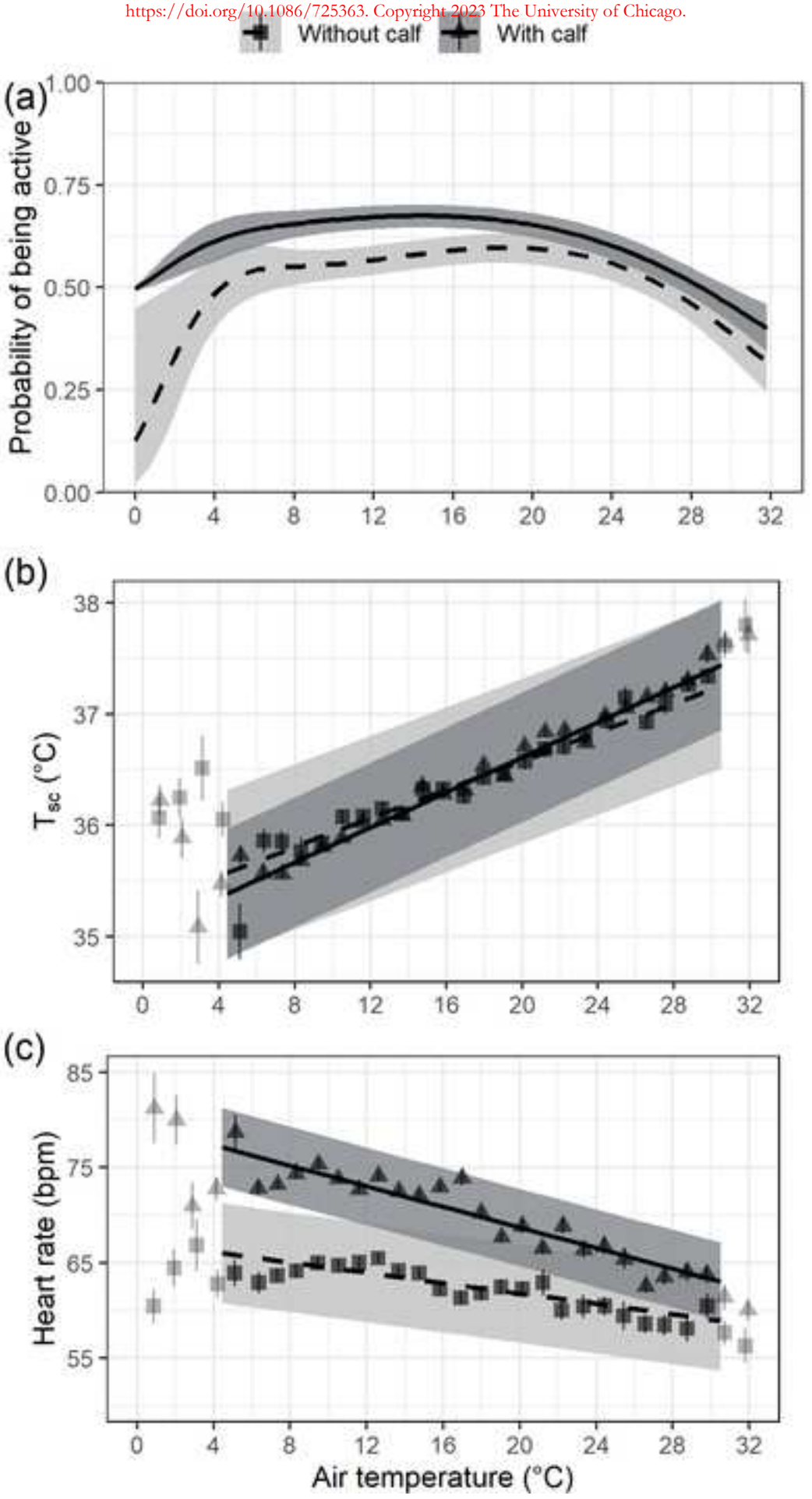

Figure 4

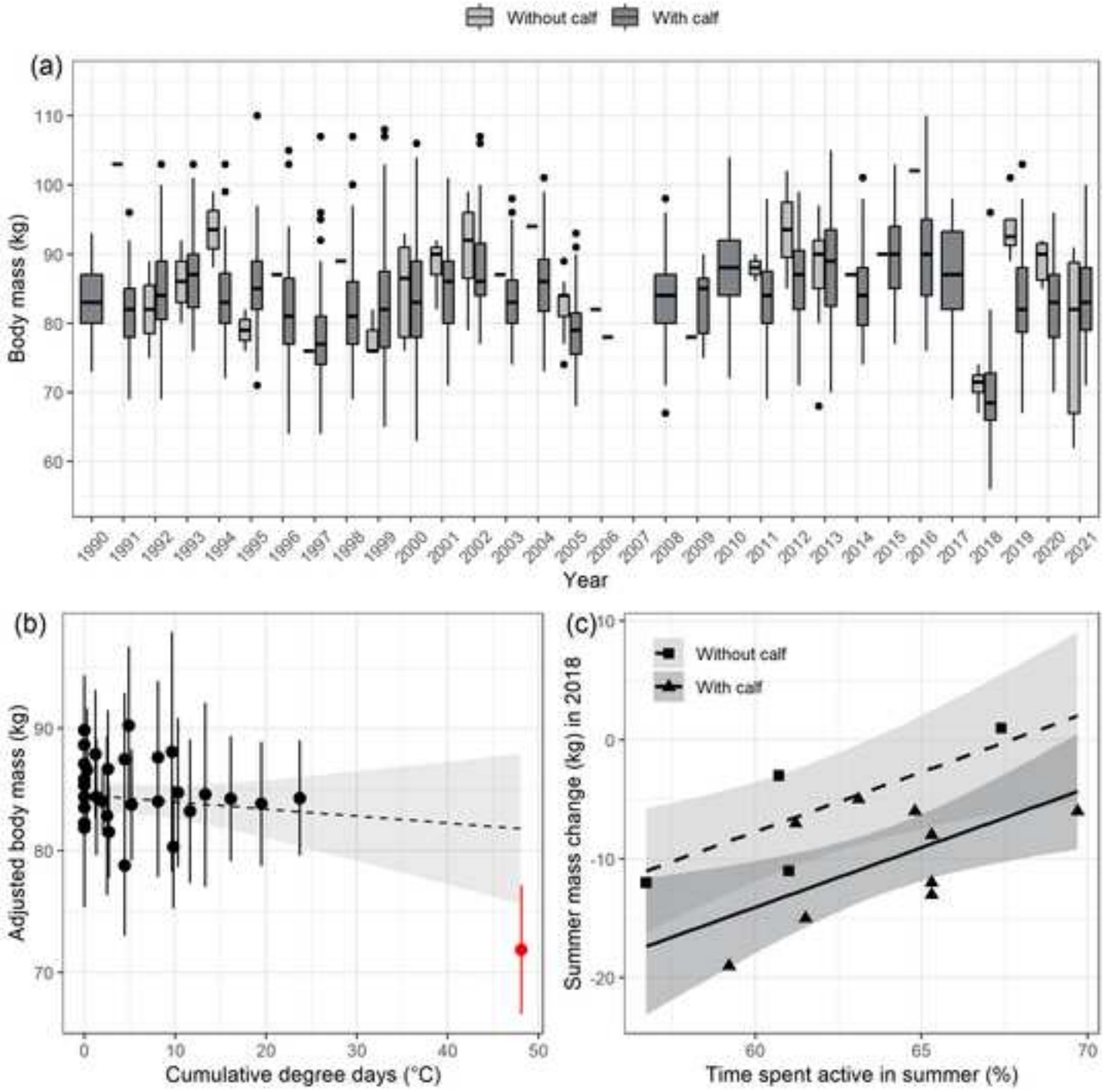

Appendix 1 for "A summer heatwave reduced activity, heart rate and autumn body mass in a cold-adapted ungulate": Additional methods and results

Contents

1 Additional methods 2
1.1 Study area 2
1.2 Biologger implantation 5
1.3 Biologger data processing 5
1.4 Hidden Markov models to assess activity patterns 6
2 Supplementary tables 12
3 Literature cited 26

1 Additional methods

1.1 Study area

The area consists mainly of open mountain birch (*Betula* spp.*)* and pine (*Pinus sylvestris*) forest or their mixture with small high open fell areas, lakes and wetlands, hence providing free access to water (Paoli et al. 2020). The region has a subarctic climate with the climatological mean (1991–2020) of air temperature (T_a) and precipitation in July (warmest month) being 14.0°C and 75 mm, respectively, and that of January (coldest month) being −11.9°C and 26 mm (Finnish Meteorological Institute 2022). The sun does not set between 17 May and 27 July, and nights remain light until ~31 August. Although the temperatures at the study site and the nearest weather station were strongly correlated (Fig. A1-2a), the difference between the daily mean temperatures at the two measurements sites was on average −1.1°C and varied by up to 2.2°C (Fig. A1-2), with the temperature at the local weather station tending to be lower than that at Ivalo Airport (site A, Fig. A1-1).

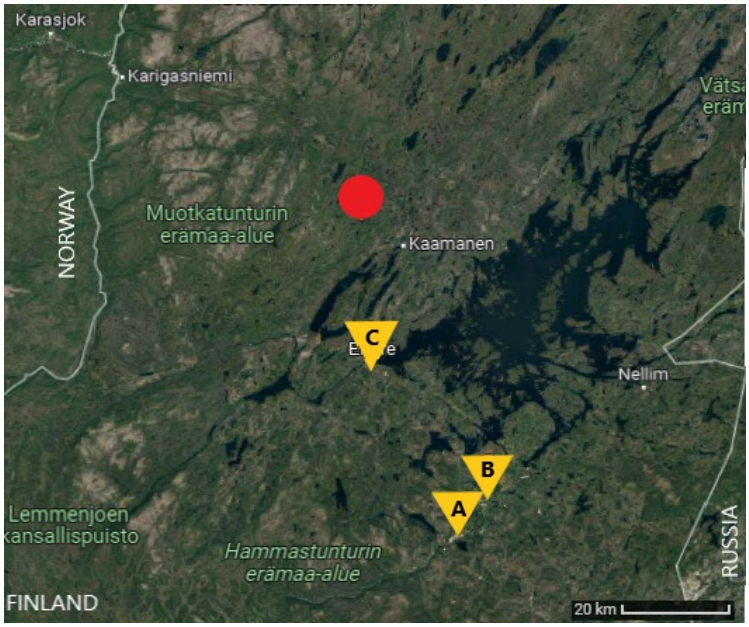

Figure A1-1. Location of study site (red circle) and weather stations from which weather data were used (yellow triangles), in Inari municipality, Finland. Station ID and distance from study area are given in parentheses. **A** – Inari Ivalo Airport (ID 102033, ~60 km). **B** – Inari Ivalo (ID 102037, ~59 km). **C** – Inari village (ID 102046, ~27 km). Precipitation data was compiled from stations B (1990–2007) and C (2007–2021). Satellite image copyright ofLandsat/Copernicus (2022), map data from Google © 2022.

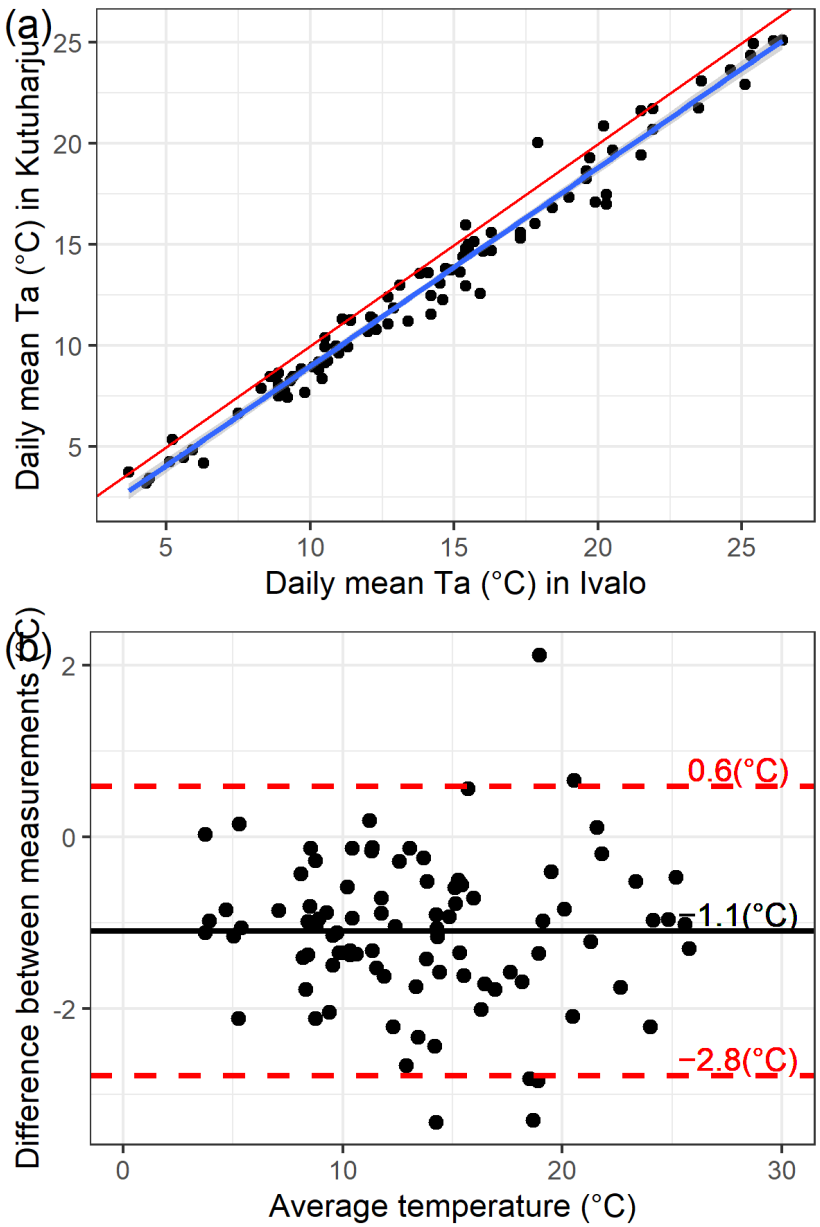

Figure A1-2. Comparison of air temperatures recorded at Inari Ivalo Airport (ID 102033, location A in Fig. A1-1), and those recorded at the study site (red circle in Fig. A1-1) during the summer 2018. (a) Daily mean air temperatures (T_a) recorded locally plotted against temperature daily mean air temperatures recorded at Inari Ivalo Airport. The red line shows a regression with slope 1 and intercept of 0, while the blue line shows the relationship between the two temperatures (slope = 0.97, SE = 0.02, $p < 0.001$, $R^2 = 0.98$). (b) Bland-Altmann plot of difference between measurements at the two sites plotted against the mean temperature from the two sites. The red dashed lines show the upper and lower limits of 95% confidence interval for the average difference between two daily mean temperatures, and the solid black line indicated the mean difference (1.1°C).

1.2 Biologger implantation

The DST centi-HRT sensors (diameter × length: 15 mm × 46 mm, mass ~19 g) were sterilised with ethylene oxide gas (Anaprolene AN74i 60 L, Andersen 60 Europe, Kortrijk, Belgium) prior to implantation. The loggers were implanted subcutaneously on the left side of the animal chest (behind the elbow). During the implantation, animals were sedated with a mix of detomidine (0.039 mg kg^{-1} BM; Domosedan vet. Orion Pharma Animal Health, Finland), ketamine (0.9 mg kg^{-1} BM; Belatamin vet., Bela-Pharm GmbH & Co, Germany) and butorphanol (0.051 mg kg^{-1} BM; Butorgesic vet. CP-Pharma Handelsgellschaft mbH, Germany) or only detomidine (0.046 mg kg^{-1} BM; Domosedan vet. Orion Pharma Animal Health, Finland) and ketamine (1.04 mg kg^{-1} BM; Belatamin vet., Bela-Pharm GmbH & Co, German), followed by administration of meloxicam (0.5 mg kg^{-1} BM; Metacam®, Boehringer Ingelheim Vetmedica GmBH, Germany) for post-operative analgesia. For local anaesthesia, we used 0.5–1 mL of bupivacaine (5 mg mL^{-1} Marcaine 5 mg mL−1, AstraZeneca, UK). The protocol for inserting the loggers has been described elsewhere (Trondrud et al. 2021). Reversal drugs were not used, and animals were kept under observation until they regained consciousness and could stand and walk on their own, which took on average 40 min post-injection and ranged from 18 min to 1 h and 23 min. Once conscious, animals were released into the calving paddock and monitored for 2 days before release into the larger winter enclosure. One year later, the loggers were retrieved using a similar procedure as described above. Ten of the 13 loggers retrieved had overlapping data with activity sensors.

1.3 Biologger data processing

Heart rate (HR) and subcutaneous temperature data (Tsc)

A raw ECG signal was stored every 6 h alongside the HR, together with a signal quality index, which we used to manually validate the recorded HR, following the method described

in Trondrud et al. (2021). Briefly, the accuracy of the internal algorithm was assessed by the goodness-of-fit of the recorded HR to the manually validated HR, with a threshold R^2 of 0.9. This was greatly reduced at values > 175 bpm for all quality levels, and in general at quality levels 1–3. Therefore, we retained only HR < 175 bpm with the quality levels 0 for further analysis. The temperature sensors measured T_{sc} with a precision of 0.032°C, with the calibration performed by the manufacturer prior to implantation. Data from the loggers were downloaded using Mercury software (StarOddi, Gardabaer, Iceland). At the time of data download, the software recorded the time in the internal clock alongside the time of the computer (in UTC). Average clock drift was 7 min 45 sec behind the computer time (range from 4 min 45 sec to 12 min 30 sec) in the loggers that were still working at the time of download. For each logger, the offset in time was corrected assuming that the drift occurred linearly. For the loggers that stopped working before download, time drifts were unavailable, and the average clock drift was used.

Accelerometery data

The clock drift was assessed by recording the exact time (in sec) when the logger was switched off (using a magnet) following retrieval from the animals. For the sensors that worked until the magnet was connected (n = 10), the mean absolute offset was 5 min (range from −10 to +3 min). One sensor had a 2-h offset, another had a 2-day offset, and two sensors stopped working several months prior to retrieval. The offset was corrected assuming a linear drift. For the loggers that stopped working prior to retrieval, the average drift of 5 min was used.

1.4 Hidden Markov models to assess activity patterns

VeDBA was modelled using a gamma distribution conditional on the underlying state. We fitted a null model with the following initial parameters representing mean and SD of the raw

data in each state: 500 ± 200 for the resting state, and 2100 ± 600 for the active state. Estimated initial parameters were then drawn from the null model and used in all subsequent models. The pseudo residuals of the model had a right-long tailed distribution (Fig. A1-4). Further model diagnostics are shown in figures A1-5 and A1-6. There was some individual variation in the distribution of VeDBA (Fig. A1-7), but the patterns were consistent with the group-level distribution used in the HMM for state assignments (Fig. A1-3).

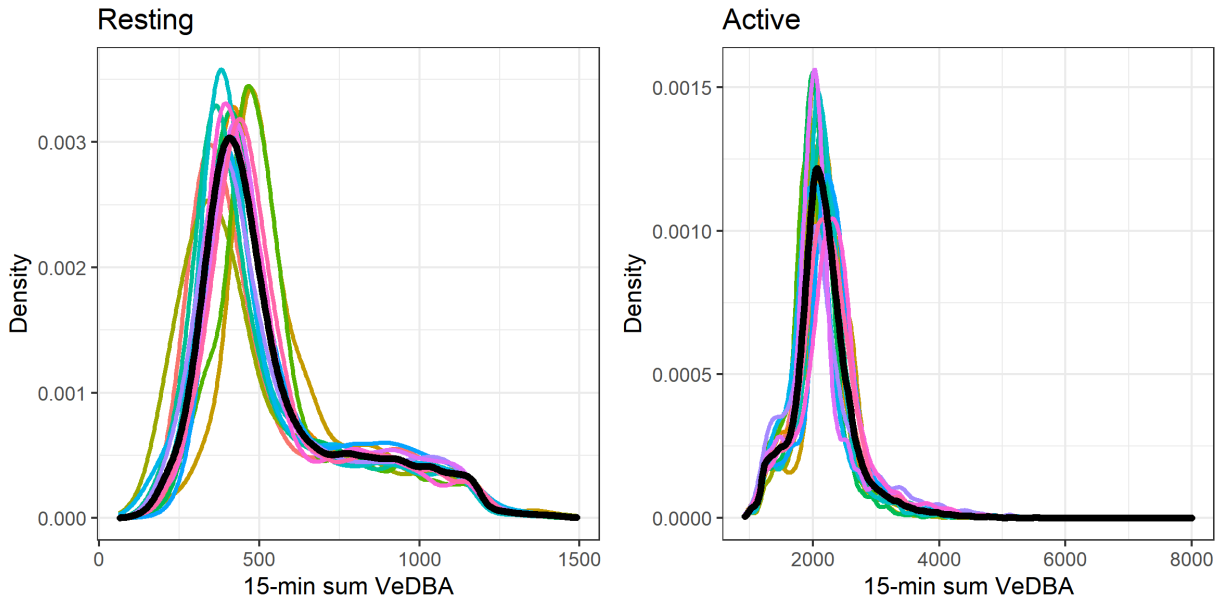

Figure A1-3. Density of sum VeDBA for all animals, categorized by state (resting/active) and shown for each individual (separated by colour). The black line shows the group-level distribution.

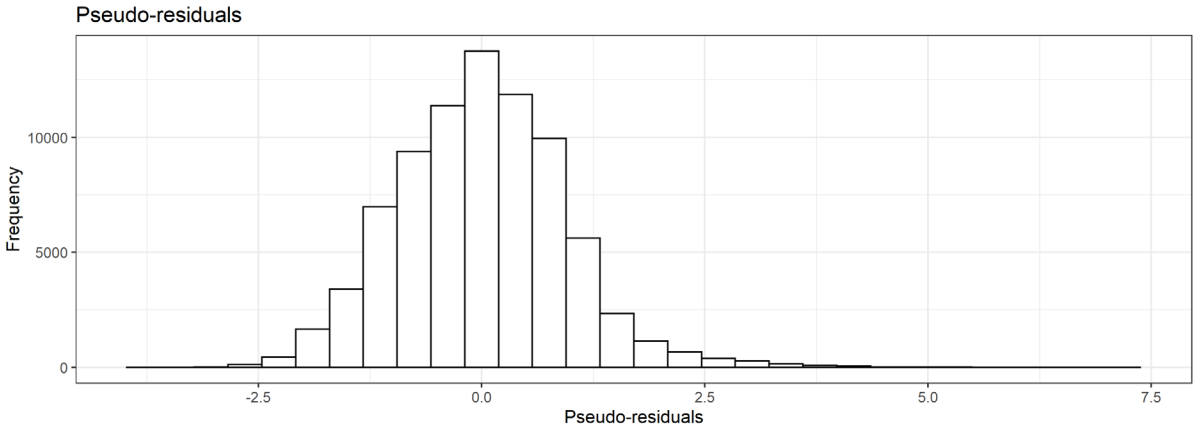

Figure A1-4. Distribution of the pseudo-residuals for the VeDBA variable included in the HMM fitted to reindeer activity data in summer.

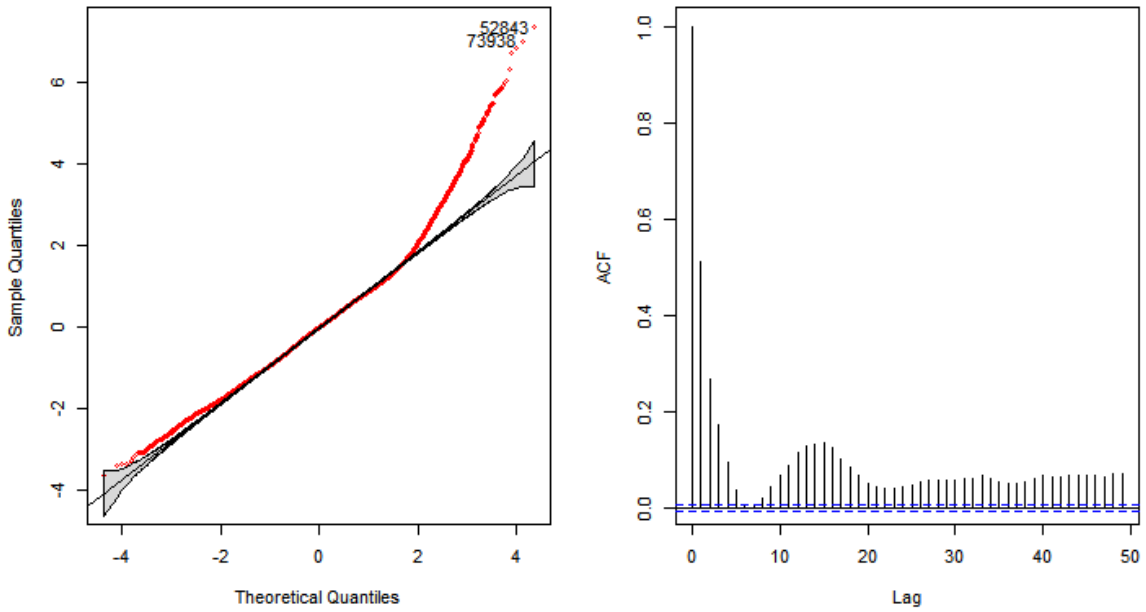

Figure A1-5. Quantile-quantile plots of the pseudo-residuals and autocorrelation function (ACF) for each consecutive time step (lag) in the activity variable VeDBA used to identify activity states in the two-state HMMs fitted to reindeer activity data in summer.

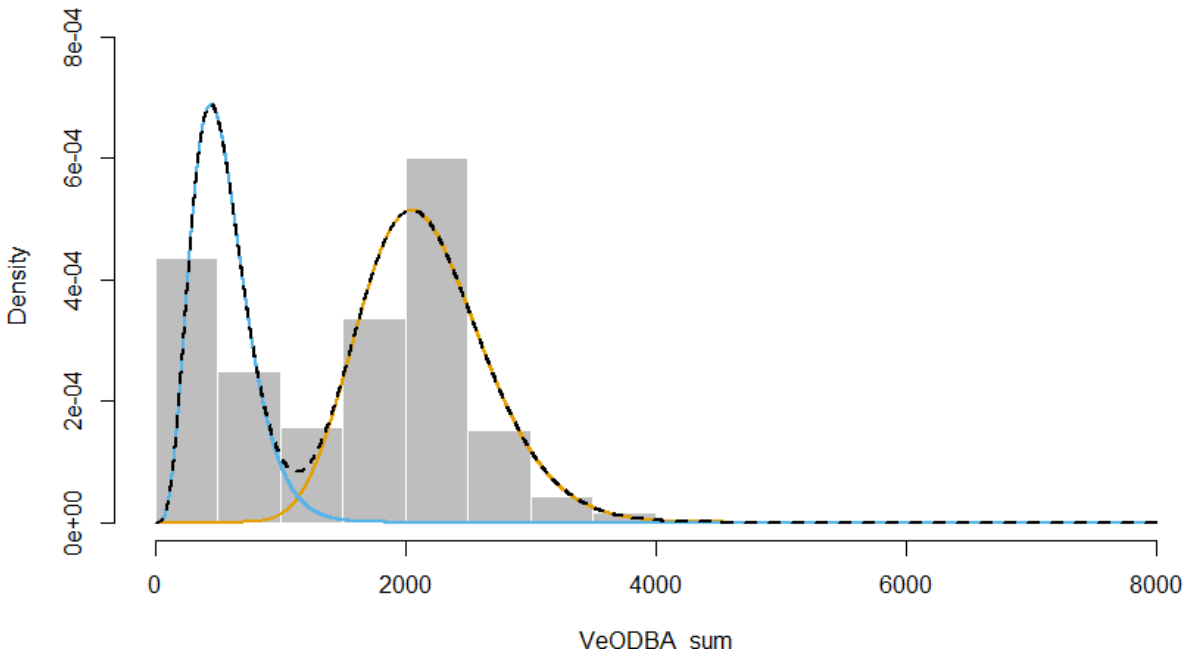

Figure A1-6. Density of sum VeDBA for all animals, categorized into inactive (blue line) and active (yellow line) by the hidden Markov model fitted to activity data for reindeer in summer.

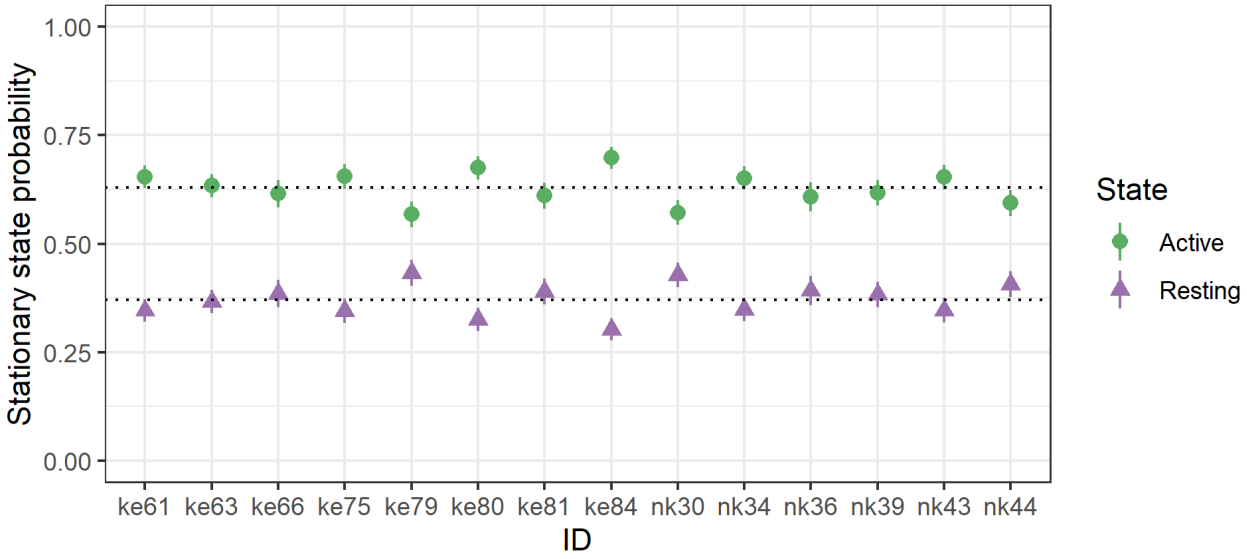

Figure A1-7. Individual−level estimates of stationary state probabilities (the probability to inhabit a given state at any time) including 95% confidence intervals for inactive (purple triangles) and active (green circles) states derived from a hidden Markov model. The dotted lines indicate the mean values for each activity state.

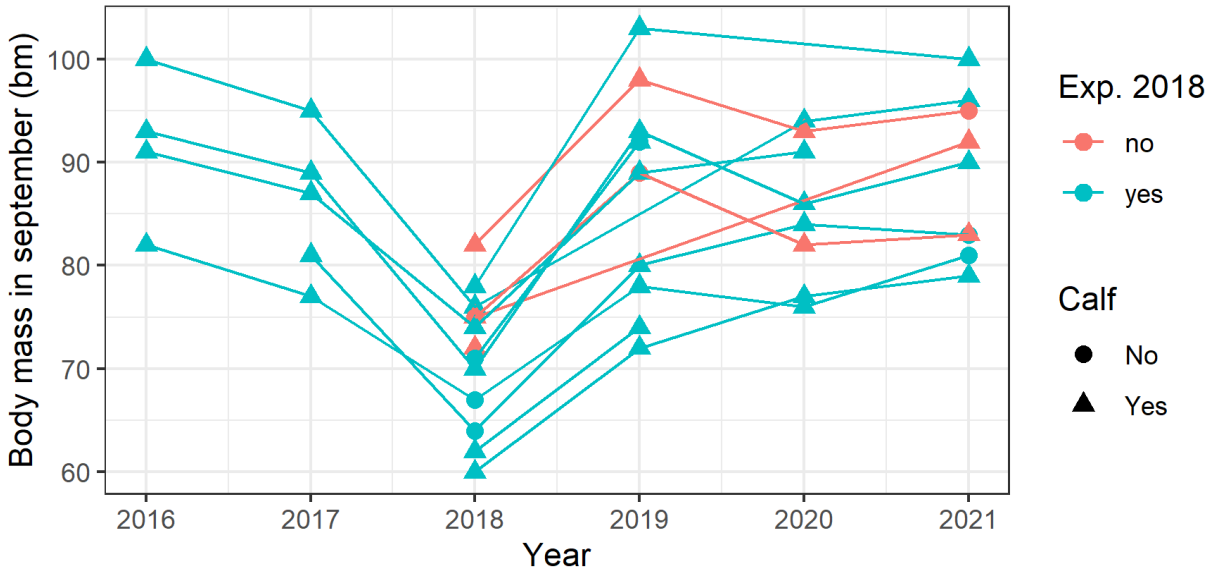

Figure A1-8. September body masses of the adult reindeer females used in this study, in the period 2016–2021. The colours indicate whether the females were a part of the experimental trial, and shapes indicate whether the females raised a calf in the given year. Each line is associated with one individual.

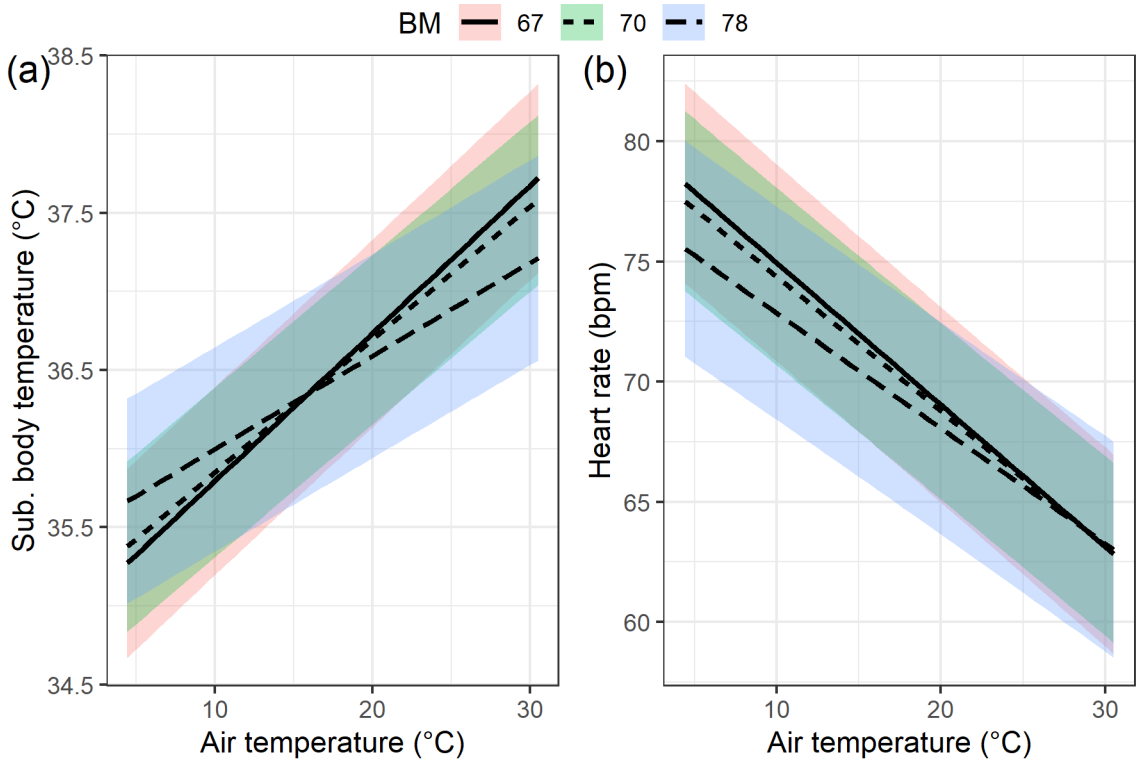

Figure A1-9. Predicted responses of adult female reindeer of three different body masses (representing the 15%, 50% and 85% quantiles) to instantaneous air temperatures from 20 June to 20 August 2018 in Kaamanen, Northern Finland. a) Subcutaneous body temperatures (T_{sc}) predicted from GAMM. b) Predicted resting heart rates predicted from GAMM. In both panels, the shaded areas show the 95% confidence interval for each prediction, and fainted points outside the prediction represent the lower 1% and upper 99% of the data. All predictions are corrected for other explanatory variables in each model.

2 Supplementary Tables

Table A1-1. Characteristics of 14 semi-domestic reindeer females with biologger data used in this study. Provided are animal ID, age (years), calf status (number of calves alive), body mass (BM) measured in April 2018 (prior to summer experiment) and in September 2018, availability of biologger data (+, yes; −, no) for heart rate (HR) subcutaneous body temperature (T_{sc}) and activity.

ID	Age (years)	Calf	BM (kg)		HR, T_{sc}	Activity data	Handled in June*
			April	Sep			
ke61	6	1	82	76	−	+	Yes
ke63	6	1	80	75	+	+	No
ke66[b]	6	2	89	82	−	+	No
ke75	5	1	73	60	+	+	Yes
ke79[a]	5	0	76	64	+	+	Yes
ke80	5	1	71	72	+	+	No
ke81[a]	5	0	78	67	+	+	Yes
ke84	5	1	68	62	−	+	Yes
nk30[a]	7	0	91	−	+	+	Yes
nk34	7	1	81	75	+	+	No
nk36	7	0	74	71	+	+	Yes
nk39	7	1	89	74	−	+	Yes
nk43	7	1	78	70	+	+	Yes
nk44	7	1	97	78	+	+	Yes

Superscripts: [a] calves were removed from mothers prior to study; [b] gave birth to twins.

*An experimental study on energy expenditure using the doubly labelled water was performed in June, during which the animals were handled daily for 7 days and kept isolated from the rest of the herd between calving (mid-May) to mid-June. During this period, the animals were supplementary fed, but there were no differences in September body between the two groups of focal animals (Welch Two Sample t-test: $t = -0.33$ $df = 3.6$, p-value = 0.76). Further details are provided in Appendix 2.

Table A1-2. Characteristics of summer weather in Northern Finland, compiled from three weather stations near our study area (Fig. A1-1). Each value is calculated across daily values reported in June, July and August for each year. Shown are the means, medians, mean daily minimum and maximum, and mean daily amplitude (difference between daily min. and max), cumulative degree days (i.e., sum of temperatures ≥ 20°C), sum of days for which daily mean air temperatures were ≥ 20°C ("hot days"), and the sum of precipitation (in mm) over summer. Data was downloaded from the Finnish Meteorological Institute (https://en.ilmatieteenlaitos.fi/download-observations/).

Year	Air temperature (°C)						Hot days	Precipitation (mm)
	Mean	Median	Mean min.	Mean max.	Mean amp.	Cumulative degree days		
1990	12.1	11.9	7.6	16.6	9	5.2	3	129.7
1991	12.1	12.8	8.1	16.5	8.5	0	0	110.8
1992	11.1	10.2	6.9	15.9	8.9	10.3	3	319.3
1993	10.6	10.1	6.9	15.1	8.2	1.2	1	200.1
1994	12.1	11.9	7.1	17.5	10.4	2.5	2	149.1
1995	11.5	11.3	7.6	16.1	8.5	0	0	292.0
1996	11.6	11.4	6.8	16.6	9.7	0	0	163.5
1997	13.3	13.5	7.9	19	11.1	4.4	7	72.2
1998	11.1	11.3	6.9	15.9	9	0	0	202.9
1999	12.3	11.7	7.8	17.1	9.3	13.3	9	284.8
2000	12.4	11.6	8.2	16.8	8.7	9.6	4	169.0
2001	12.6	12.8	8.2	17.3	9.1	4.4	1	249.0
2002	13.1	13.5	8.7	17.9	9.2	0	0	228.4
2003	12.8	12.2	8.4	17.2	8.8	16.1	12	201.2
2004	13.1	13.4	8.5	17.6	9.1	2.6	5	239.7
2005	13.5	13.6	9.1	18.1	9	9.8	5	242.1
2006	13.4	13.7	8.7	18.3	9.7	2.7	2	134.3
2007	12.2	12.5	8.3	16.8	8.5	4.3	2	217.1
2008	10.7	10.2	7	14.8	7.8	0	0	211.8
2009	12.1	12.2	8.1	16.4	8.3	2	1	209.6
2010	12	12.3	8.2	16.4	8.2	0	0	251.5
2011	12.9	12.6	8.3	17.8	9.5	11.6	7	219.2
2012	11.2	10.9	6.9	15.7	8.8	0	0	203.3
2013	14.4	14.2	9.9	19.3	9.5	8.1	6	85 1
2014	13.5	12.8	9.4	18.2	8.8	23.7	11	187.8
2015	11.3	10.7	7.4	15.4	7.9	0	0	169.5
2016	12.8	12.9	8.8	17	8.2	4.9	4	331.0
2017	11.5	12.1	7.4	15.7	8.3	0.3	1	299.4
2018	14.2	13.9	9.7	19	9.3	48.1	16	231.9
2019	11.5	10.6	7.5	15.9	8.5	8.1	4	196.0
2020	13.4	13.2	9	18.2	9.2	1.3	2	187.5
2021	13.8	13	9.3	18.5	9.2	19.5	10	212.9

Table A1-3. Body mass statistics of semi-domestic reindeer females who had a calf in the current year, for the years 1990–2021. Blank space indicates missing data for a given month/year. The range shows the lowest and highest body mass recorded in the given month, and sample sizes (unique individuals each month/year) are given in parentheses.

	Body mass in April (kg)		Body mass in September (kg)	
Year	Mean ± SD	Range (n)	Mean ± SD	Range (n)
1990	83.9 ± 5.8	72–100 (57)	83.6 ± 5.3	73–93 (39)
1991	80.1 ± 7	64–96 (62)	82.2 ± 6.2	69–96 (37)
1992	85.6 ± 9.3	62–107 (63)	85.2 ± 7	69–103 (43)
1993	82 ± 10	59–105 (66)	87 ± 5.8	76–103 (54)
1994	90.5 ± 8.9	68–109 (55)	83.8 ± 7.3	72–103 (34)
1995	84.1 ± 10.3	59–117 (68)	85 ± 6.9	71–110 (52)
1996	83.5 ± 9.4	58–113 (65)	81.7 ± 8.1	64–105 (51)
1997	81.8 ± 8.9	62–111 (76)	77.9 ± 7.6	64–107 (73)
1998	79 ± 8	65–104 (80)	82.1 ± 7.4	69–107 (81)
1999	77.8 ± 10.4	55–109 (81)	83.2 ± 9.3	65–108 (79)
2000	78 ± 8.8	67–86 (6)	83.7 ± 8.8	63–106 (138)
2001	75.6 ± 9.2	60–107 (65)	85.4 ± 6.9	71–101 (67)
2002	80.8 ± 7.1	67–99 (69)	87.6 ± 6.3	77–107 (67)
2003	80.4 ± 7.5	58–100 (67)	83.6 ± 5.5	74–98 (64)
2004	82.6 ± 6.5	66–103 (74)	85.9 ± 5.8	73–101 (72)
2005	82.2 ± 5.6	70–94 (61)	79 ± 5.5	68–93 (55)
2006	75 ± NA	75–75 (1)	78 ± NA	78–78 (1)
2007				
2008	87.5 ± 7.3	66–100 (60)	82.9 ± 7.6	54–98 (54)
2009	83.9 ± 9	73–95 (8)	82.9 ± 5.7	75–90 (7)
2010	87.3 ± 9	69–107 (53)	87.9 ± 7.4	72–104 (47)
2011	87.8 ± 7.8	72–105 (51)	83.8 ± 7.3	69–98 (39)
2012	89.4 ± 7.8	77–106 (47)	86.4 ± 7	71–99 (43)
2013	86.1 ± 8.9	68–106 (42)	88 ± 7.9	70–105 (35)
2014	87 ± 8	74–111 (60)	84.4 ± 6.3	74–101 (56)
2015	86.4 ± 7.6	73–107 (57)	90 ± 6	77–103 (41)
2016	87.6 ± 7.5	73–103 (37)	90.4 ± 8	76–110 (33)
2017	87.5 ± 6.8	73–102 (54)	86.4 ± 7.1	69–98 (48)
2018	78.9 ± 8.1	55–97 (57)	69.6 ± 6.7	56–96 (50)
2019	84.5 ± 6.7	69–100 (66)	82.7 ± 7.1	67–103 (60)
2020	82.1 ± 6.1	70–98 (138)	83.1 ± 5.9	70–96 (106)
2021	84.1 ± 8.4	68–106 (136)	83.6 ± 6.2	71–100 (114)
Summary	**83.3 ± 8.7**	**55–117 (1882)**	**83.7±7.8**	**54–110 (1740)**

Table A1-4. Body mass statistics of semi-domestic reindeer females who did not have a calf in the current year, for the years 1990–2021. Blank space indicates missing data for a given month/year. The range shows the lowest and highest body mass recorded in the given month, and sample sizes are given in parentheses.

	Body mass in April (kg)		Body mass in September (kg)	
Year	Mean ± SD	Range (n)	Mean ± SD	Range (n)
1990				
1991	83	83 (1)	103	103(1)
1992	81 ± 17	69–93 (2)	82 ± 9.9	75–89 (2)
1993	82.5 ± 9.2	76–89 (2)	86 ± 8.5	80–92 (2)
1994	87 ± 4.2	84–90 (2)	93.5 ± 7.8	88–99 (2)
1995	73 ± 4.2	70–76 (2)	79 ± 4.2	76–82 (2)
1996	77	77–77 (1)	87	87 (1)
1997	66	66–66 (1)	76	76 (1)
1998	74	74–74 (1)	89	89–89 (1)
1999	65.3 ± 4.7	60–69 (3)	78 ± 3.5	76–82 (3)
2000			85.2 ± 6.7	76–93 (12)
2001	72.4 ± 9.9	62–84 (5)	88.4 ± 4	82–92 (5)
2002	72 ± 5.9	66–78 (4)	90.5 ± 8.7	79–99 (4)
2003	85 ± NA	85–85 (1)	87 ± NA	87–87 (1)
2004	72.5 ± 3.5	70–75 (2)	94 ± NA	94–94 (1)
2005	74.1 ± 6.9	65–84 (10)	82.4 ± 4.6	74–89 (9)
2006	80	80 (1)	82	82 (1)
2007				
2008				
2009	79.5 ± 14.8	69–90 (2)	78	78 (1)
2010	88	88 (1)		
2011	80.3 ± 8.1	71–85 (3)	88 ± 2.8	86–90 (2)
2012	78.2 ± 11.9	66–95 (6)	93.5 ± 7.2	85–102 (4)
2013	77.6 ± 9	66–96 (9)	86.9 ± 8.8	68–97 (9)
2014	84 ± 7	76–89 (3)	87	87 (1)
2015	80.7 ± 10	73–92 (3)	90	90 (1)
2016				
2017	79 ± 11.3	71–87 (2)	102	102 (1)
2018	74 ± 0	74–74 (2)	70.7 ± 3.5	67–74 (3)
2019	86 ± 1.8	84–88 (4)	93.8 ± 5.1	89–101 (4)
2020	83.2 ± 6.1	76–92 (8)	89 ± 3.2	85–92 (6)
2021	73.1 ± 11.8	51–86 (16)	78.3 ± 13.3	62–91 (6)
Summary	**77.1 ± 3.4**	**51–96 (97)**	**85.8 ± 8.5**	**62–103 (86)**

Table A1-5. AIC model selection for hidden Markov models used to identify state occupancy (inactive/active) from the sum VeDBA at 15 min resolution in 14 adult reindeer females. The different models are fitted with the same initial parameters (drawn from the null model) for two underlying states. In each model, additional variables to explain transition and stationary state probabilities are included. TempCat, 5-level temperature category for mean daily air temperatures; Calf, factor indicating if female was with (1) or without (0) calf, Time of day, numeric value indication hour of the day (0–24 hrs); Air temp., 2 m air temperature recorded from local weather station; ID, individual identifier.

Formula	Delta	w
Air temp. × Calf + time of day + ID	0	0.74
TempCat × time of day	2	0.26
Air temp. + time of day + ID	19	0.00
Air temp. + time of day + Calf + ID	23	0.00
Air temp. + time of day	160	0.00
Air temp. + ID	215	0.00
Air temp. + Calf + ID	219	0.00
Air temp. × Calf + ID	220	0.00
TempCat + time of day	231	0.00
Time of day	278	0.00
Air temp. + Calf	299	0.00
Air temp.	336	0.00
Calf + ID	403	0.00
Calf	482	0.00
Temp. category	488	0.00
Null	520	0.00
ID	520	0.00
TempCat × time of day + ID	1760	0.00
TempCat × time of day + Calf + ID	1795	0.00
TempCat + time of day + ID	2066	0.00
TempCat + time of day + Calf + ID	2070	0.00
Time of day + ID	3004	0.00
Time of day + calf + ID	3008	0.00
TempCat + time of day + Calf	8316	0.00
Time of day + calf	30855	0.00

Table A1-6. Model selection results using generalized linear mixed-effects model with subcutaneous body temperature and heart rate while resting as the response variable (in separate models), individual as random effect and an autoregressive to account for within-individual temporal autocorrelation. Presented is the model structure, the likelihood ratio value (L. ratio), change in degrees of freedom (ΔDF) between original and reduced models, as well as the P-value indicating the significance level of the given change in model fit. The top model (in bold) is the one presented in the main results. Here the abbreviated parameters refer to: HR, heart rate, T_{sc}, subcutaneous body temperature; VeDBA, vectorial dynamic body acceleration; BM, body mass; ID, individuals; calf, calf status; T_a , air temperature ; day, calendar day; TOD, time of day.

Model parameters		L. ratio	ΔDF	P
Subcutaneous body temperature				
2	HR + VeDBA+BM + Calf + Ta + BM×Ta+Calf×Ta+S (Day)+S(TOD)+S (ID)	0.39	1	0.53
1	HR + VeDBA+ Age+BM+Calf+Ta+BM × Ta+Calf × Ta+S(Day)+S(TOD)+S (ID)			
Heart rate				
2	Tsc + VeDBA+BM + Calf + Ta + BM×Ta+Calf×Ta+S (Day)+S(TOD)+S (ID)	3.08	1	0.08
1	Tsc + VeDBA+ Age+BM+Calf+Ta+BM × Ta+Calf × Ta+S(Day)+S(TOD)+S (ID)			

Table A1-7. Parameter estimates of the best-fit GAMM using subcutaneous body temperature (T_{sc}) as the response variable, in 10 adult female reindeer while inactive. T_{sc} was modelled as a function of age, body mass (BM) measured in September, calf status (0 = no calf, 1 = with calf), heart rate (HR), activity level (VeDBA), and air temperature (T_a). Calendar day was fitted with a thin-plate regression spline, time of day (ToD) was fitted with a cubic circular regression and individual was fitted as random intercept. All numeric variables were scaled to a mean of 0 and standard deviation equal to 1 prior to modelling. Provided are the model predictor names, estimates, 95% confidence intervals (CI), estimated degrees of freedom (EDF), which represents curvature of the smoothing parameter (the higher the number, the more variation), p-values for the smooth terms, total number of observations and the adjusted R^2 of the model.

Predictors	**Estimates**	**CI**	**P-value**
(Intercept)	35.98	35.33, 36.63	<0.001
HR	−0.05	−0.07, −0.03	<0.001
VeDBA	−0.32	−0.39, −0.26	<0.001
BM	0.01	−0.31, 0.34	0.942
Calf [1]	−0.08	−0.91, 0.76	0.859
T_a	0.40	0.36, 0.43	<0.001
BM × T_a	−0.11	−0.12, −0.09	<0.001
Calf [1] × T_a	0.09	0.06, 0.12	<0.001
Smooth terms	**EDF**	**F**	**P-value**
S (Day)	8.49	52.31	<0.001
S (Time of day)	5.58	17.50	<0.001
S (ID)	6.99	706.86	<0.001
Observations	17217		
Adj. R^2	0.341		

Table A1-8. Parameter estimates of the best-fit GAMM using heart rate (HR) as the response variable, in 10 adult female reindeer. The final model included the following explanatory variables: body mass (BM) measured in September, calf status (0 = no calf, 1 = with calf), subcutaneous body temperature (T_{sc}), activity level (VeDBA), and air temperature (T_a). Calendar day was fitted with a thin-plate regression spline, time of day (ToD) was fitted with a cubic circular regression and individual was fitted as random intercept. All numeric variables were scaled to a mean of 0 and standard deviation equal to 1 prior to modelling. Provided are the model predictor names, estimates, 95% confidence intervals (CI), estimated degrees of freedom (EDF), which represents curvature of the smoothing parameter (the higher the number, the more variation), p-values for the smooth terms, total number of observations and the adjusted R^2 of the model.

Predictors	**Estimates**	**CI**	**P-value**
(Intercept)	66.37	61.88, 70.86	<0.001
VeDBA	3.06	2.23, 3.89	<0.001
BM	−0.76	−2.97, 1.45	0.501
Calf [1]	8.31	2.64, 13.98	0.004
T_{sc}	−0.53	−0.75, −0.31	<0.001
T_a	−1.69	−2.12, −1.26	<0.001
BM × T_a	0.35	0.16, 0.54	<0.001
Calf [1] × T_a	−1.67	−2.08, −1.25	<0.001
Smooth terms	**EDF**	**F**	**P-value**
S (Day)	8.07	76.16	<0.001
S (Time of day)	4.76	10.79	<0.001
S (ID)	6.95	184.08	<0.001
Observations	17217		
Adj. R^2	0.24		

Table A1-9. Parameter estimates of generalised additive mixed-effects model using September body mass (kg) in adult (> 2 years old) female reindeer (N = 344) for the years 1990 to 2021. Here, body mass is modelled as a function of April body mass (centred to mean of 0), calf status in summer (0 – no calf, 1 – calf), and smoothed terms for age (thin-plate regression spline), ID (random intercept) and year (random intercept). Provided are the model predictor names, estimates, 95% confidence intervals (CI), estimated degrees of freedom (EDF), which represents curvature of the smoothing parameter (the higher the number, the more variation), p-values for the smooth terms, total number of observations and the adjusted R^2 of the model.

Predictors	Estimate	CI	P-value
(Intercept)	87.17	85.48 – 88.86	<0.001
Calf [1]	−3.90	−4.72 – −3.08	<0.001
April body mass	1.92	1.52 – 2.31	<0.001
Smooth terms	**EDF**	**F**	**P-value**
S (age)	4.7	13.1	<0.001
S (ID)	312.4	14.2	<0.001
S (year)	28.5	178.7	<0.001
Observations	1519		
Adj. R^2	0.815		
Deviance explained (%)	85.7		

Table A1-10. Model selection using Akaike's information criteria for small sample sizes (AICc), where September body mass (n = 1519, N_{id} = 344) is fitted as the response variable in a generalized additive model. All models contained the following variables: April body mass in the current year, age (fitted as a spline with 10 knots), calf status (factor) and individual and year fitted as random intercepts, separately. This is the base model shown in Table A8. In addition, the models tested included environmental variables shown and described in Table A2. Shown are the model numbers, formula (not showing the base structure of the intercept model), number of fixed parameters (k), AICc score, delta AICc, the AIC weight, log-likelihood of the model and total estimated degrees of freedom (EDF) for the smoothed parameters.

Model	Formula	df	AICc	Delta	Weight	Log-likelihood	EDF
m6	Cumulative temp.	3	8541.4	0.0	0.18	-3817.2	348.1
m5	Hot days + Precipitation	3	8542.0	0.6	0.13	-3816.2	348.8
m4	Hot days	3	8542.0	0.7	0.13	-3816.1	348.9
m7	Cumulative temp. + Precipitation	3	8542.2	0.8	0.12	-3815.9	349.0
m8	Mean temp.+ Hot days	3	8542.3	0.9	0.11	-3816.3	348.8
m2	Mean temp.	3	8542.5	1.1	0.10	-3816.4	348.9
m9	Mean temp. + Precipitation	3	8542.8	1.5	0.09	-3816.2	349.1
m3	Precipitation	3	8543.0	1.7	0.08	-3816.8	348.8
m1	Base	3	8543.2	1.9	0.07	-3816.2	349.2

Table A1-11. Parameter estimates of the best-fit model from AIC model selection in Table A10. Here, adult female reindeer body mass in September is modelled as a function of April body mass (centred to mean of 0), calf status in summer (0 – no calf, 1 – calf), cumulative degree days in summer (sum of daily temperatures above 20°C) and smoothed terms for age (thin-plate regression spline), ID (random intercept) and year (random intercept). Provided are the model predictor names, estimates, 95% confidence intervals (CI), estimated degrees of freedom (EDF), which represents curvature of the smoothing parameter (the higher the number, the more variation), p-values for the smooth terms, total number of observations and the adjusted R^2 of the model.

Predictors	Estimate	CI	P-value
(Intercept)	87.15	85.61 – 88.68	<0.001
Calf [1]	-3.91	-4.73 – -3.09	<0.001
April body mass	1.92	1.53 – 2.32	<0.001
Smooth terms	**EDF**	**F**	**P-value**
S(Cumulative temp.)	2.4	6.5	0.001
S (age)	4.5	14.2	<0.001
S (ID)	312.4	10.5	<0.001
S (year)	25.7	99.2	<0.001
Observations	1519		
Adj. R^2	0.815		
Deviance explained (%)	85.7		

Table A1-12. Parameter estimates of generalised additive mixed−effects model using September body mass (kg) of reindeer calves (n = 1427) for the years 1990 to 2021. Here, body mass is modelled as a function of mother's April body mass (centred to mean of 0), sex (0 – female, 1 – male), and smoothed terms for mother's age (thin−plate regression spline) and ID (random intercept), as well as year of birth (random intercept). Provided are the model predictor names, estimates, 95% confidence intervals (CI), estimated degrees of freedom (EDF), which represents curvature of the smoothing parameter (the higher the number, the more variation), p−values for the smooth terms, total number of observations and the adjusted R^2 of the model.

Predictors	Estimate	CI	P−value
(Intercept)	43.45	41.86 – 45.05	<0.001
Birthweight	1.33	1.06 – 1.60	<0.001
Sex [M]	3.28	2.85 – 3.71	<0.001
Body mass of mother	1.93	1.58 – 2.29	<0.001
Smooth terms	**EDF**	**F**	**P−value**
S (age of mother)	7.35	3.60	<0.001
S (ID)	126.43	0.91	<0.001
S (year)	29.0	50.95	<0.001
Observations	1427		
Adj. R^2	0.661		
Deviance explained (%)	70.1%		

Table A1-13. Model selection using Akaike's information criteria for small sample sizes (AICc), where September body mass of calves (n = 1427) is fitted as the response variable in a generalized additive model. All models contained the following variables: mother's April body mass (centred to mean of 0), sex (0 – female, 1 – male), and smoothed terms for mother's age (thin−plate regression spline) and ID (random intercept), as well as year of birth (random intercept). This is the base model shown in Table A9. In addition, the models tested included environmental variables shown and described in Table A2. Shown are the model numbers, formula (not showing the base structure of the intercept model), number of fixed parameters (k), AICc score, delta AICc, the AIC weight, log-likelihood of the model and total estimated degrees of freedom (EDF) for the smoothed parameters.

Model	Formula	df	AICc	Delta	Weight	Log-likelihood	EDF
m6	Cumulative temp.	4	8029.5	0.0	0.15	-3826.4	165.3
m2	Mean temp.	4	8029.7	0.1	0.14	-3825.5	166.0
m8	Mean temp. + Precipitation	4	8029.8	0.3	0.13	-3825.5	166.1
m7	Cumulative temp. + Precipitation	4	8029.9	0.3	0.12	-3827.6	164.5
m4	Hot days	4	8029.9	0.3	0.12	-3825.1	166.5
m1	Base	4	8030.0	0.5	0.12	-3824.7	166.8
m5	Hot days + Precipitation	4	8030.1	0.5	0.11	-3825.0	166.6
m3	Precipitation	4	8030.2	0.7	0.11	-3824.6	166.9

Table A1-14. Model selection using Akaike's information criteria for small sample sizes (AICc), where the body mass change from April to September in 2018) is fitted as the response variable in a simple linear regression, against summer activity levels and calf status. Shown are the formulas, degrees of freedom (df), AICc score, delta AICc and the AIC weights of each model.

Formula	k	df	AICc	Delta	Weight	Log-likelihood
Mean activity + calf	3	10	83.5	0.0	0.35	-35.3
Intercept	1	12	84.9	1.4	0.18	-39.8
Mean activity	2	11	85.1	1.6	0.16	-38.2
Mean activity on hot days	2	11	85.6	2.1	0.12	-38.5
Calf	2	11	86.7	3.2	0.07	-39.0
Mean activity on hot days + calf	3	10	86.8	3.3	0.07	-36.9
Diff. activity on hot days	2	11	87.6	4.1	0.05	-39.5
Diff. activity on hot days + calf	3	10	89.9	6.4	0.01	-38.4

3 Literature cited

Finnish Meteorological Institute. 2022. Temperature and precipitation statistics from 1961 onwards.

Paoli A., R.B. Weladji, Ø. Holand, and J. Kumpula. 2020. Early-life conditions determine the between-individual heterogeneity in plasticity of calving date in reindeer. (J. Gaillard, ed.)J Anim Ecol 89:370–383.

Trondrud L.M., G. Pigeon, S. Albon, W. Arnold, A.L. Evans, R.J. Irvine, E. Król, et al. 2021. Determinants of heart rate in Svalbard reindeer reveal mechanisms of seasonal energy management. Philos Trans R Soc B Biol Sci 376:20200215.

Appendix 2 for "A summer heatwave reduced activity, heart rate and autumn body mass in a cold-adapted ungulate":

Additional analyses comparing the two groups used in the study

Contents

1.Activity 1
2. Subcutaneous body temperature (T_{sc}) and heart rate (HR) 4
3. September body mass 10

This appendix outlines a set of statistical analyses used to compare responses between the animals in the focal group (n = 14) that were part of a doubly labelled water (DLW) experiment prior to the present study (n = 10) and those that were not (n =4).

Activity

To assess whether the two DLW groups differed in activity levels or response to air temperature, we first ran an HMM including *only* whether the animals belonged to the DLW group (n = 10) or not (n = 4) as a factor. Here, we found that there was a small, but significant, difference in the stationary state probabilities (probability to be either active or resting) between the groups (Table A2-1, Fig A2-1a). We therefore re-ran the 5 HMMs of best fit (Table A1-5) together with their base models and compared these with and without a factor indicating whether the animals belonged to the doubly labelled water (DLW) group (n =10) or not (n = 4). Because all females without a calf belonged to the DLW group, we ran all HMMs with either calf status or DLW group as an explanatory variable. We then compared with AIC model selection and found that a model containing the DLW group as an *additive* effect outperformed that including calf status (Table A2-2). However, the uncertainty around the estimates for the two groups was large with overlapping credible intervals (CrI). Since no other analyses show that there are significant differences between these groups (detailed below), we argue against including this as an explanatory variable. We believe that our argument is strengthened when we evaluate the individual probability estimates and see that the individual-level estimates for the animals that were not handled in June do not clearly separate from the mean, and the model estimates including DLW group as a covariate is likely pulled by the one individual with relatively high activity levels (Fig. A2-2).

Table A2-1. Stationary state probabilities estimated from a Hidden Markov model with only DLW group as the explanatory variable (0-not handled, 1-handled in June), for resting and active states. Shown are the probability estimates and lower and upper 95% credibility intervals.

Exp. Group	State	Stationary state probability	lower 95% CrI	upper 95% CrI
0	Resting	0,36	0,34	0,37
1	Resting	0,38	0,37	0,39
0	Active	0,64	0,63	0,66
1	Active	0,62	0,61	0,63

Table A2-2. AIC model selection for hidden Markov models used to identify state occupancy (inactive/active) from the sum VeDBA at 15 min resolution in 14 adult reindeer females. The selected models include the top 5 of the original AIC model selection (Table A2-5) and their base models. For each, we included a model accounting for whether the animals were handled in June or not ('DLW). Shown for each model are the model formula, delta AIC, weights, and number of parameters (k).

Formula	Delta	Weight	k
Airtemp. + time of day + DLW + ID	0	1	20
Airtemp. × calf + time of day + ID	27	0	23
TempCat × time of day	29	0	14
Airtemp. × DLW + time of day + ID	31	0	23
Airtemp + time of day + ID	45	0	19
Airtemp. + time of day + calf + ID	49	0	20
Airtemp. + time of day + DLW	183	0	7
Airtemp. + DLW + ID	246	0	18
Airtemp. + Calf + ID	246	0	18
time of day	305	0	2
Airtemp.	363	0	4
Airtemp.× DLW	363	0	4
ID	425	0	13
ID+DLW	429	0	14
Calf	509	0	1
TempCat	515	0	4
DLW	545	0	1
null	546	0	0

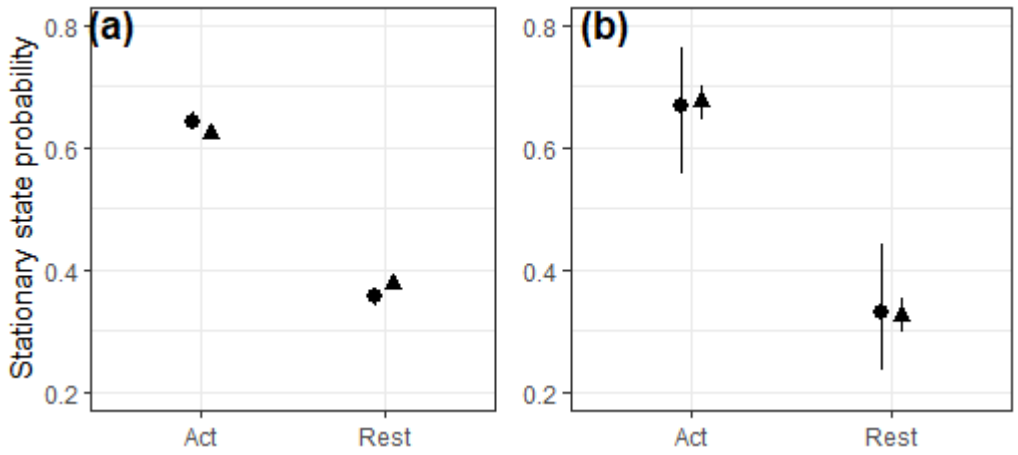

Figure A2-1. Estimated stationary state probabilities for animals that were handled in June (triangles, n = 10) and animals that were not handled in June (circles, n = 4), derived from a) an HMM object containing DLW group as the only covariate, and b) the best-fit HMM object including DLW group as an additive effect. Bars indicate 95% credible intervals.

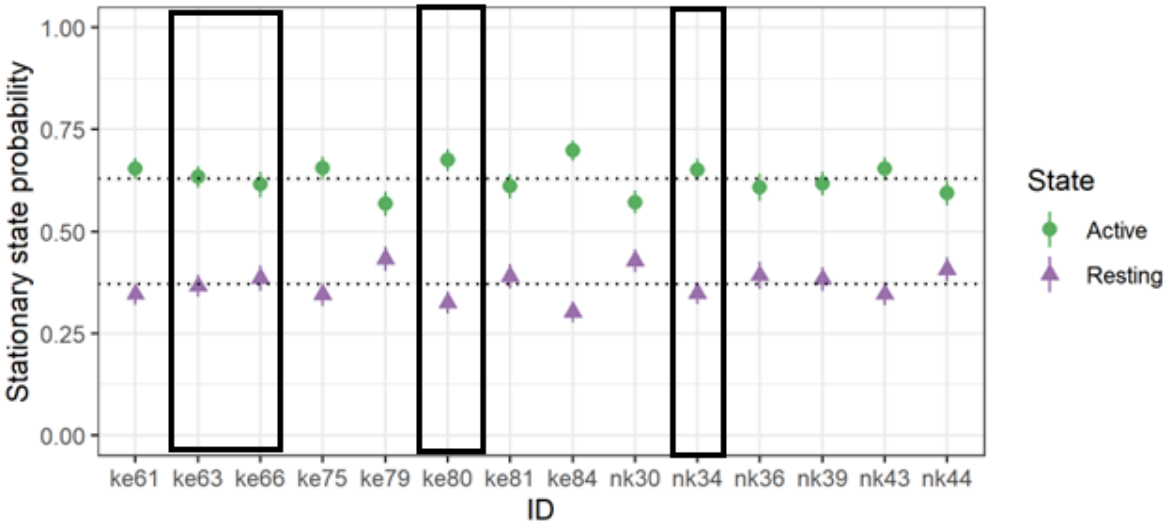

Figure A2-2. Estimated stationary state probabilities for each individual derived from an HMM object containing ID as a covariate. The individuals that were not handled in June are emphasized by the black rectangles.

Subcutaneous body temperature (T_{sc}) and heart rate (HR)

In the heart rate and body temperature datasets, we had only 3 individuals that did not undergo the DLW experiment (one had missing data), and all three had a calf (Table A2-3). We did not find an additive effect of DLW treatment on subcutaneous body temperature (Table A2-4), but when including DLW group in an interaction with temperature, we found a significant effect (Table A2-5). For heartrate neither the additive effect (Table A2-6) nor the interaction with air temperature was significant (Table A2-7). However, because the DLW group now contained 7 individuals of which 4 that did not have a calf, we are not sure if this difference is pulled by the response of the barren females. We could not fit calf status and DLW group in an interaction as there were no females without a calf in the non-experiment group. We therefore compared the two models with AIC. Here, were found that for both subcutaneous body temperature and heart rate, the original models were a better fit than those including an interaction between DLW group and air temperature (Table A2-8).

Table A2-3. Overview of each' individuals calf status (0 – no calf, 1 - calf) and DLW group (0 – no DLW, 1- DLW) for the animals with available activity, heart rate and body temperature data (n = 10).

Animal ID	Calf in 2018	DLW in June 2018
ke63	1	0
ke75	1	1
ke79	0	1
ke80	1	0
ke81	0	1
nk30	0	1
nk34	1	0
nk36	0	1
nk43	1	1
nk44	1	1

Table A2-4. Parameter estimates of generalized additive mixed-effects model using subcutaneous body temperature (T_{sc}) as the response variable (revision of Table A1-6 in Appendix 1). Here, we included a factor indicating whether the animal was intensively handled in June ('DLW'), highlighted in yellow. T_{sc} was modelled as a function of age, body mass (BM) measured in September, calf status (0 = no calf, 1 = with calf), heart rate (HR), activity level (VeDBA), and air temperature (T_a). Calendar day was fitted with a thin-plate regression spline, time of day (ToD) was fitted with a cubic circular regression and individual was fitted as random intercept. All numeric variables were scaled to a mean of 0 and standard deviation equal to 1 prior to modelling. Provided are the model predictor names, estimates, 95% confidence intervals (CI), estimated degrees of freedom (EDF), which represents curvature of the smoothing parameter (the higher the number, the more variation), p-values for the smooth terms, total number of observations and the adjusted R^2 of the model.

		temp	
Predictors	*Estimates*	*CI*	*p*
(Intercept)	36.40	34.71 – 38.10	<0.001
DLW [1]	-0.46	-1.81 – 0.88	0.499
HR	-0.05	-0.07 – -0.03	<0.001
VeDBA	-0.32	-0.39 – -0.26	<0.001
Age	-0.07	-0.70 – 0.56	0.819
BM	0.02	-0.55 – 0.59	0.947
Calf [1]	-0.29	-1.48 – 0.89	0.629
T_a	0.40	0.36 – 0.43	<0.001
BM × T_a	-0.11	-0.12 – -0.09	<0.001
Calf [1] × T_a	0.09	0.06 – 0.12	<0.001
Smooth terms	**EDF**	**F**	**P-value**
S (Day)	8.48	52.31	<0.001
S (Time of day)	5.58	14.94	<0.001
S (ID)	4.99	694.90	<0.001
Observations	17217		
R^2	0.34		

Table A2-5. Parameter estimates of generalized additive mixed-effects model using subcutaneous body temperature (T_{sc}) as the response variable (revision of Table A1-6 in Appendix 1). Here, we included a factor indicating whether the animal was intensively handled in June ('DLW'), and an interaction between 'exp' and air temperature. The interaction between calf status and air temperature is removed due to the variables being mutually exclusive. T_{sc} was modelled as a function of age, body mass (BM) measured in September, calf status (0 = no calf, 1 = with calf), heart rate (HR), activity level (VeDBA), and air temperature (T_a). Calendar day was fitted with a thin-plate regression spline, time of day (ToD) was fitted with a cubic circular regression and individual was fitted as random intercept. All numeric variables were scaled to a mean of 0 and standard deviation equal to 1 prior to modelling. Provided are the model predictor names, estimates, 95% confidence intervals (CI), estimated degrees of freedom (EDF), which represents curvature of the smoothing parameter (the higher the number, the more variation), p-values for the smooth terms, total number of observations and the adjusted R^2 of the model.

		temp	
Predictors	*Estimates*	*CI*	*p*
(Intercept)	36.39	34.70 – 38.09	<0.001
DLW [1]	-0.46	-1.81 – 0.89	0.503
HR	-0.05	-0.07 – -0.03	<0.001
VeDBA	-0.32	-0.38 – -0.25	<0.001
Age	-0.08	-0.71 – 0.55	0.803
BM	0.02	-0.55 – 0.60	0.932
Calf [1]	-0.28	-1.46 – 0.90	0.642
T_a	0.42	0.38 – 0.46	<0.001
BM × T_a	-0.09	-0.10 – -0.07	<0.001
DLW [1] × T_a	0.05	0.01 – 0.09	0.006
Smooth terms	**EDF**	**F**	**P-value**
S (Day)	8.47	52.92	<0.001
S (Time of day)	5.58	15.85	<0.001
S (ID)	4.99	592.75	<0.001
Observations	17217		
R^2	0.341		

Table A2-6. Parameter estimates of generalized additive mixed-effects model using **heart rate** (HR) as the response variable (revision of Table A1-6 in Appendix 1). Here, we included a factor indicating whether the animal was intensively handled in June ('DLW'), highlighted in yellow. HR was modelled as a function of age, body mass (BM) measured in September, calf status (0 = no calf, 1 = with calf), heart rate (HR), activity level (VeDBA), and air temperature (T_a). Calendar day was fitted with a thin-plate regression spline, time of day (ToD) was fitted with a cubic circular regression and individual was fitted as random intercept. All numeric variables were scaled to a mean of 0 and standard deviation equal to 1 prior to modelling. Provided are the model predictor names, estimates, 95% confidence intervals (CI), estimated degrees of freedom (EDF), which represents curvature of the smoothing parameter (the higher the number, the more variation), p-values for the smooth terms, total number of observations and the adjusted R^2 of the model.

		Heart rate	
Predictors	*Estimates*	*CI*	*p*
(Intercept)	69.58	57.54 – 81.63	<0.001
DLW [1]	-2.71	-12.27 – 6.85	0.578
VeDBA	3.06	2.23 – 3.89	<0.001
Age	0.90	-3.55 – 5.36	0.691
BM	-1.53	-5.59 – 2.52	0.458
Calf [1]	6.74	-1.67 – 15.15	0.116
T_{sc}	-0.53	-0.75 – -0.31	<0.001
T_a	-1.69	-2.12 – -1.25	<0.001
BM × T_a	0.35	0.16 – 0.54	<0.001
Calf [1] × T_a	-1.67	-2.08 – -1.25	<0.001
Smooth terms	**EDF**	**F**	**P-value**
S (Day)	8.07	76.18	<0.001
S (Time of day)	4.76	9.18	<0.001
S (ID)	4.98	235.88	<0.001
Observations	17217		
R^2	0.247		

Table A2-7. Parameter estimates of generalized additive mixed-effects model using heart rate (HR) as the response variable (revision of Table A1-7 in Appendix 1). Here, we included a factor indicating whether the animal was intensively handled in June ('DLW'), and an interaction between 'exp' and air temperature. The interaction between calf status and air temperature is removed due to the variables being mutually exclusive. HR was modelled as a function of age, body mass (BM) measured in September, calf status (0 = no calf, 1 = with calf), heart rate (HR), activity level (VeDBA), and air temperature (T_a). Calendar day was fitted with a thin-plate regression spline, time of day (ToD) was fitted with a cubic circular regression and individual was fitted as random intercept. All numeric variables were scaled to a mean of 0 and standard deviation equal to 1 prior to modelling. Provided are the model predictor names, estimates, 95% confidence intervals (CI), estimated degrees of freedom (EDF), which represents curvature of the smoothing parameter (the higher the number, the more variation), p-values for the smooth terms, total number of observations and the adjusted R^2 of the model.

		Heart rate	
Predictors	*Estimates*	*CI*	*p*
(Intercept)	69.82	57.83 – 81.81	<0.001
DLW [1]	-2.85	-12.36 – 6.66	0.557
VeDBA	3.04	2.21 – 3.87	<0.001
Age	1.02	-3.42 – 5.46	0.653
BM	-1.63	-5.67 – 2.40	0.428
Calf [1]	6.52	-1.85 – 14.89	0.127
T_{sc}	-0.56	-0.79 – -0.34	<0.001
T_a	-2.49	-2.96 – -2.02	<0.001
DLW × T_a	-0.43	-0.90 – 0.03	0.069
BM × T_a	0.08	-0.11 – 0.27	0.422
Smooth terms	**EDF**	**F**	**P-value**
S (Day)	8.11	75.80	<0.001
S (Time of day)	4.72	8.54	<0.001
S (ID)	4.98	195.42	<0.001
Observations	17217		
R^2	0.245		

Table A2-8. AIC model selection for 1) subcutaneous body temperature and 2) heart rate comparing models with or without DLW group as a factor variable and in interaction with air temperature. The tables refer to the corresponding tables showing the parameter estimates of each model. Shown are degrees of freedom and ΔAIC.

	df	ΔAIC
1) Subcutaneous body temperature		
Calf model (Table A2-4)	15	0
DLW model (Table A2-5)	15	21
2) Heart rate		
Calf model (Table A2-6)	14	0
DLW model (Table A2-7)	14	58

September body mass

With respect to the long-term body mass analyses, we ran all the models with and without the DLW group, as well as included the DLW treatment as a factor variable in the model for long-term body mass. Within 2018, the body mass of the DLW manipulated animals (n = 10) was on average 70 kg, while the average body mass of the remaining 4 focal animals was 72 kg, but these body masses did not differ significantly (Welch Two Sample t-test: $t = -0.33$ df = 3.6, p-value = 0.76). Due to the low sample size, we could not account for April body mass or calf status in this comparison.

For all animals weighed in September 2018 (n = 52), we compared the body masses of the DLW group (n = 10) against the remaining individuals (n = 42) including the other four in the focal group using a regression model (same GAM structure as described in the manuscript on lines 196-200). We accounted for calf status, age and April body mass in a gam, and fitted body mass in September to the DLW group as a factor, showing that the body masses of the DLW group were not significantly different from the rest (Table A2-9). Then we compared the body masses of the focal group (n = 14) against the remaining individuals (n = 38) in September 2018. Using the same approach as above, we demonstrated that the body masses of the focal group did not differ significantly from the rest of the herd in 2018 (TableA2-10), which we believe justifies our inclusion of this group in the long-term analyses of body mass.

Table A2-9. Parameter estimates of generalized additive mixed-effects model using September body mass (kg) in adult (> 2 years old) female reindeer (n = 52) in 2018. Here, body mass is modelled as a function of whether the animals had been handled in June in 2018 (DLW = TRUE) in addition to April body mass (centred to mean of 0), calf status in summer (0 – no calf, 1 – calf), and smoothed terms for age (thin-plate regression spline), ID (random intercept) and year (random intercept). The other focal animals (n=4) are excluded from the model. Provided are the model predictor names, estimates, 95% confidence intervals (CI), estimated degrees of freedom (EDF), which represents curvature of the smoothing parameter (the higher the number, the more variation), p-values for the smooth terms, total number of observations and the adjusted R2 of the model.

Predictors	*Estimates*	*CI*	*p*
(Intercept)	75.94	72.28 – 79.61	<0.001
Calf [TRUE]	-3.46	-7.05 – 0.13	0.059
DLW [TRUE]	-2.52	-5.96 – 0.91	0.146
bm april (scaled)	0.55	0.37 – 0.74	<0.001
Smooth terms	**EDF**	**F**	**P-value**
S (age)	3.07	4.19	0.005
Observations	53		
R^2	0.59		

Table A2-10. Parameter estimates of generalized additive mixed-effects model using September body mass (kg) in adult (> 2 years old) female reindeer (n = 52) in 2018. Here, body mass is modelled as a function of whether they had had a biologger implanted in 2018 (Focal = TRUE) in addition to April body mass (centred to mean of 0), calf status in summer (0 – no calf, 1 – calf), and smoothed terms for age (thin-plate regression spline), ID (random intercept) and year (random intercept). Provided are the model predictor names, estimates, 95% confidence intervals (CI), estimated degrees of freedom (EDF), which represents curvature of the smoothing parameter (the higher the number, the more variation), p-values for the smooth terms, total number of observations and the adjusted R2 of the model.

Predictors	*Estimates*	*CI*	*p*
(Intercept)	74.78	70.88 – 78.68	<0.001
Calf [TRUE]	-2.69	-6.41 – 1.03	0.152
Focal [TRUE]	0.20	-2.96 – 3.36	0.898
bm april (scaled)	0.55	0.36 – 0.74	<0.001
Smooth terms	**EDF**	**F**	**P-value**
S (age)	3.07		0.007
Observations	53		
R^2	0.573		